의학박사 학위논문

# Fibroblast-derived CCL3 promotes prostate cancer progression by inhibiting the PLZF expression

# 섬유아세포 유래 CCL3에 의한 PLZF 발현 억제가 전립선암 진행에 미치는 기전

2022년 2월

서울대학교 대학원

의과학과 의과학전공

노 금 희

A thesis of the Degree of Doctor of Philosophy

# Fibroblast-derived CCL3 promotes prostate cancer progression by inhibiting the PLZF expression

## 섬유아세포 유래 CCL3에 의한 PLZF 발현 억제가 전립선암 진행에 미치는 기전

February 2022

The Department of Biomedical Sciences,
Seoul National University
College of Medicine

Kum Hee Noh

# Fibroblast-derived CCL3 promotes prostate cancer progression by inhibiting the PLZF expression

지도 교수 예 상 규

이 논문을 의학박사 학위논문으로 제출함
2021년 10월

서울대학교 대학원
의과학과 의과학전공
노 금 희

노금희의 의학박사 학위논문을 인준함
2022년 1월

위 원 장 _____ (인)

부위원장 _____ (인)

위 원 _____ (인)

위 원 _____ (인)

위 원 _____ (인)

# Fibroblast-derived CCL3 promotes prostate cancer progression by inhibiting the PLZF expression

by

Kum Hee Noh

A thesis submitted to the Department of Biomedical Science in partial fulfillment of the requirements for the Degree of Doctor of Philosophy in Biomedical Science at Seoul National University College of Medicine

October 2021

Approved by Thesis Committee:
January 2022

| | | |
|---|---|---|
| Chair | _____ | (Seal) |
| Vice Chair | _____ | (Seal) |
| Examiner | _____ | (Seal) |
| Examiner | _____ | (Seal) |
| Examiner | _____ | (Seal) |

# ABSTRACT

# Fibroblast-derived CCL3 promotes prostate cancer progression by inhibiting the PLZF expression

Kum Hee Noh
The Department of Biomedical Sciences
The Graduate School
Seoul National University

Prostate cancer is the most common carcinoma in men, but it is difficult to detect early because it has few symptoms. It has been reported that if the metastasis progresses to the stage where it is accompanied by pain, the survival rate is significantly lower than in the initial stage even if it is discovered. Therefore, the importance of strategies to suppress the metastasis of prostate cancer is emerging, and it is important to find a breakthrough target to be used for early detection. Consequently, I attempted to analyze the mechanism of inhibiting the metastasis of prostate cancer by various substrate cells in the tumor microenvironment.

In this study, it was confirmed that promyelocytic leukemia zinc finger (PLZF) expression not only showed a negative correlation with persistently STAT3 overexpressing high-grade prostate

cancer patient tissue, but also contributed to the patient's prognosis. Also, knockdown of PLZF promoted proliferation, inhibited apoptosis, and accelerated the migration and invasion of human prostate cancer cells.

However, although PLZF is a transcription factor, a question arises as it cannot regulate the transcription of STAT3, an oncogene, and only reduces tyrosine phosphorylation. So, I hypothesized that PLZF in prostate cancer cell lines might be related to tyrosine phosphatase, which reduces the phosphorylation of Janus kinases (JAKs)−STAT3. As a result, PLZF acts as a transcription factor of SHP−1 among various tyrosine phosphatases, thereby proving a novel regulator role in repressing the JAKs−STAT3 mechanism. These results were confirmed that SHP−1, like PLZF, is associated with prognosis in prostate cancer patient tissues.

Through the interaction between substrate cells in the tumor microenvironment and prostate cancer cells, I tried to find the reason why PLZF, a tumor suppressing gene, is suppressed in prostate cancer. These results suggest that the collapse of PLZF expression by the C-C motif chemokine ligand 3 (CCL3) derived from fibroblasts accelerates the cell migration and invasion properties of prostate cancer cells through the exchange of signaling substances between cancer cells and fibroblast.

In conclusion, prostate cancer cells inhibit PLZF signaling pathway through fibroblasts−derived CCL3, suggesting that PLZF can be a new treatment strategy to inhibit tyrosine phosphorylation through SHP−1. It is expected that PLZF could be a remarkable target for prostate cancer therapy.

Keyword : PLZF, SHP-1, JAK-STAT3, Prostate cancer, Fibroblast, Tumor suppressor gene

Student Number : 2014-21996

# CONTENTS

Abstract ..... i

Contents ..... iv

List of figures ..... v

List of abbreviations ..... viii

INTRODUCTION ..... 1

MATERIAL AND METHODS ..... 5

RESULTS ..... 15

FIGURES ..... 26

DISCUSSION ..... 72

REFERENCES ..... 77

ABSTRACT IN KOREAN ..... 91

# LIST OF FIGURES

Figure 1. PLZF expression negatively correlates with high-grade prostate cancer patient tissue and STAT3 activation ..... 26

Figure 2. PSA patterns of PLZF and STAT3 activation levels in prostate cancer patient tissues ..... 28

Figure 3. PLZF expression inversely correlates with survival in prostate cancer patients ..... 29

Figure 4. PLZF inhibits tyrosine phosphorylation of STAT3 in prostate cancer cell lines ..... 31

Figure 5. PLZF does not affect total STAT3 expression or protein-protein binding with STAT3 ..... 32

Figure 6. PLZF reduces tyrosine phosphorylation, not serine phosphorylation, of STAT3 in both cytosol and nucleus ..... 34

Figure 7. PLZF decreases prostate cancer cell viability ..... 35

Figure 8. PLZF induces G0/G1 phase arrest in prostate cancer cell lines ..... 37

Figure 9. PLZF induces apoptosis in prostate cancer cell lines ..... 39

Figure 10. PLZF and knockdown of STAT3 decrease the migration in DU145 cells ..... 41

Figure 11. PLZF reduces the migration and invasion ability in prostate

cancer cell lines ..... 43

Figure 12. PLZF diminished ECM degradation as evidenced by decreased levels of MMP9 and MMP11 ..... 46

Figure 13. PLZF inhibits the tyrosine phosphorylation of JAKs-STAT signaling ..... 47

Figure 14. PLZF inhibits the tyrosine phosphorylation of JAKs-STAT3 signaling by increasing SHP-1 ..... 48

Figure 15. PLZF suppresses tyrosine phosphorylation of JAK-STAT3 signaling by increasing SHP-1 ..... 50

Figure 16. PLZF increases the transcriptional activity of SHP-1 ... 51

Figure 17. SHP-1 expression positively correlates with PLZF expression, and negatively correlates with high-grade GS and PSA pattern in prostate cancer patient tissues ..... 52

Figure 18. LNCaP cells co-cultured with fibroblasts inhibited PLZF most clearly among various stromal cells in the tumor microenvironment ..... 54

Figure 19. Schematic of the experimental set-up for conditioned media (CMs) treatment and the transwell co-culture system ..... 55

Figure 20. Protein and RNA expression of PLZF more reduce by direct co-culturing of fibroblast ..... 56

Figure 21. Conditioned media associated with fibroblast promotes

prostate cancer cell proliferation ..... 57

Figure 22. Conditioned media associated with fibroblast promotes the migration and invasion ability in prostate cancer cell lines by inhibiting PLZF ..... 58

Figure 23. Fibroblasts affect PLZF and pY-STAT3 expressions of prostate cancer cells and non-prostate normal cells ..... 60

Figure 24. Fibroblast-induced effect was practically abolished by heat inactivation..... 61

Figure 25. Identification of tumor associated fibroblast-derived cytokines..... 62

Figure 26. Fibroblasts visibly induced CCL3 and uPAR mRNA production by co-culturing with prostate cancer cells..... 65

Figure 27. Blocked CCL3 abolished the effect of PLZF caused by fibroblast..... 66

Figure 28. SHP-1-driven transcription is more inhibited with Co-CM than FCM by CCL3 ..... 68

Figure 29. Blockade of CCL3 inhibited the fibroblast-induced migration and invasion of cancer cells..... 69

Figure 30. The mechanism of PLZF as a tumor suppressor in prostate cancer progression ..... 71

# LIST OF ABBREVIATIONS

ADT: Androgen deprivation therapy

BCL-xL: B-cell lymphoma-extra large

BCL-2: B-cell lymphoma-2

CAF: Cancer associated fibroblast

CCK: Cell counting kit

CCL3: C-C motif chemokine ligand 3

CM: Conditioned media

CRPC: Castration resistant prostate cancer

ECM: Extracellular matrix

EMT: Epithelial-mesenchymal transition

GS: Gleason score

HDF: Human dermal fibroblast

IHC: Immunohistochemistry

JAK: Janus kinase

PCNA: Proliferating cell nuclear antigen

PI: Propidium iodide

PLZF: Promyelocytic leukemia zinc finger

PSA: Prostate specific antigen

qRT-PCR: Quantitative real-time polymerase chain reaction

STAT3: Signal transducer and activator of transcription 3

TCGA: The cancer genome atlas

uPAR: Urokinase-type plasminogen activator receptor

ZBTB16: Zinc finger and BTB domain-containing 16

# INTRODUCTION

Prostate cancer is the most frequently diagnosed malignancies and the sixth leading cause of cancer-related death in men worldwide [1]. In general, patients with organ-confined prostate cancer are treated successfully. However, uncontrolled metastasis indicates disease relapse, which is virtually incurable and results in considerable disease mortality [2-4]. In addition, although much research has been done to determine the cause of prostate cancer metastasis, our understanding is still incomplete. For this reason, a better understanding of prostate cancer metastasis would lead to new approaches and targets for preventing or treating metastasis [5].

Tumors can be considered as complex organs composed of tumor cells and various non-malignant stromal cells that form the tumor microenvironment. These stromal cells include endothelial cells, pericytes, immune inflammatory cells, and fibroblasts, all of which are genetically stable and typically not malignant [6-8]. However, they are affected by interactions with tumor cells via soluble factors and modify tumor cells to favor tumor development, tumor growth, and invasion [8-10]. Among them, fibroblasts are crucial regulators of prostate tumor metastatic progression [11,12]. Several researches have investigated that the normal fibroblasts have a role in maintaining epithelial homeostasis by inhibiting the proliferation and carcinogenic potential of the adjacent epithelium; but, following

neoplastic transformation of the epithelium, cancer-associated fibroblasts (CAFs) promote tumor growth and remodels the extracellular matrix (ECM). That is, normal fibroblasts can be trained by carcinoma cells to become CAFs [13-15].

The mechanism by which local prostate cancer progresses into a lethal disease is unclear. One predictable mechanism is the loss or alteration of tumor-suppressor genes. PLZF, also known as zinc finger and BTB domain-containing 16 (*ZBTB16*), binds to specific DNA sequences with its carboxyl-terminal zinc finger domain and protein-protein interaction [16,17]. PLZF is involved in diverse cellular signaling, particularly in stem cells self-renewal or differentiation, hematopoiesis, and immune regulation [18-22]. Lately, PLZF was reported to potentially play a tumor-suppressor role, which reduces cell growth and survival in numerous solid tumors, including melanoma, malignant mesothelioma, and non-small cell lung cancer cells [23-26]. Besides, recent studies also suggested that PLZF is implicated in prostate cancer as a tumor-suppressor protein. In prostate cancer, PLZF expression is reduced or lost in high grade tumor and castration-resistant prostate cancer (CRPC) [17,27]. PLZF inhibits prostate cancer cell growth through its inhibitory effects on AR, AKT, mTOR, and MAPK signaling [28,29]. Research of PLZF is actively underway as it has a high potential as a target for prostate cancer, but the relationship between prostate tumor microenvironment and PLZF is not yet well known. Therefore, I aim to clarify the role of PLZF in the association between prostate cancer and the tumor microenvironment. Restoring PLZF expression or

reactivation also could be a novel strategy for prostate cancer therapy.

CCL3, which belongs to the C–C chemokine family, is produced by fibroblast, macrophage, T cell, monocytes, and epithelial cells. CCL3, also known as macrophage inflammatory protein 1$\alpha$ (MIP−1$\alpha$), is a pro−inflammatory cytokine and is a ligand for CCR5, which stimulates chemotactic activities in a variety of immune cells such as monocytes, lymphocytes, macrophages [30,31]. CCL3 has also been involved in the regulation of cancer cell growth, angiogenesis and metastasis of various tumors such as melanoma, colorectal cancer, and renal cell carcinoma [32]. Previously, several evidence models suggested that fibroblast−derived CCL3 could activate tumor progression. Deficiency of the CCL3/CCR5 system resulted in a remarkably decreased tumor formation and lung metastasis. CCL3/CCR5 accumulation of CAFs also have been reported to be important in colitis−related carcinogenesis and oral tumor formation [32−35]. However, the fundamental mechanisms of CCL3 in the tumor microenvironment and the signaling pathways are not well known.

In this study, I hypothesized that PLZF is suppressed by fibroblasts that interacted with cancer, thereby promoting metastatic prostate cancer progression. As a result, I found that tumor−induced impetus stimulated fibroblasts to produce CCL3, which promoted prostate cancer growth and metastasis through the reduction of PLZF/tyrosine phosphatase SHP−1. By studying the PLZF/SHP−

1/STAT3 signaling pathway involved in CCL3-induced malignancy, I may find a potential therapeutic target for prostate cancer.

# MATERIALS AND METHODS

## Cell culture and culture conditions

The human prostate cancer cell line (LNCaP) was purchased from the Korean Cell Line Bank (Seoul, Republic of Korea). Another human prostate cancer cell line (DU145) and normal human dermal fibroblast cell line (HDF) were kindly provided by the German Collection of Microorganisms (DSMZ, Braunschweig, Germany) and Modern Cell & Tissue Technologies (Seoul, Republic of Korea). The normal prostate epithelial cells (PNT2), lymphocytes (Jurkat-T), NK cells (NK-92) and monocytes (THP-1) were purchased from American Type Culture Collection (Manassas, VA, USA). DU145 cells was maintained in Dulbecco's Modified Eagles media (Capricorn scientific, Germany). LNCaP, PNT2, Jurkat-T, NK-92, THP-1 and normal HDF cells were maintained in RPMI-1640 media (Life Technologies, Carlsbad, CA, USA). All the cells were maintained in the media supplemented with 10% heat-inactivated fetal bovine serum (FBS, Life Technologies) and 1% penicillin/streptomycin solution (Life Technologies) at 37℃ with 5% $CO_2$ in a humidified incubator.

## Conditioned media preparation and cell co-culture

Conditioned media (CM) was prepared by incubating normal HDF, Jurkat-T, NK-92 and THP-1 cells in 10 mL per 100 mm dish for 48 h with RPMI-1640 media (Life Technologies) containing only 1% penicillin/streptomycin solution (Life Technologies). Supernatant was collected and centrifuged at 13000 rpm for 3 min to remove the cell debris. Cells were cultured with the CMs mixed with an equal volume of fresh media for 24 h.

To observe cell interactions between the two cells, cells were seeded at the same density ($5 \times 10^5$ cells per well) into 6-well plates (SPL, Gyeonggi, Republic of Korea) and other cells were seeded into the upper chamber of a 0.4-μm co-culture chamber (Corning Inc. Corning, NY, USA). The co-culture chambers were then inserted into the plate wells. After 24 h of co-culture, cells at the plate bottom were harvested and used in the experiments.

## Immunohistochemistry (IHC) staining and scoring

Briefly, the arrays were rehydrated and autoclaved at 121℃ for 10 min in a citrate buffer (Fisher Scientific, Rockford, IL, USA) to retrieve antigen. They were incubated with 3% $H_2O_2$ for 10 min and with 10% bovine serum for 1 h to block non-specific signals. Sections were incubated overnight at 4℃ with antibodies against PLZF (1:200; AbCam, Cambridge, UK), pY-STAT3 (1:50; Cell Signaling Technology, Danvers, MA, USA), and SHP-1 (1:200; AbCam). Immune complexes were visualized using the Vectastatin

ABC kit (Vector Laboratories, Burlingame, CA, USA) and the DAB detection kit (Dako, Carpinteria, CA, USA). Finally, all sections were counterstained with hematoxylin. Positive staining cells were counted on 5 randomly chosen visual fields at 400× magnification by means of Image J (National Institutes of Health, Bethesda, MD, USA)

### Human prostate cancer patient tissues

Human prostate cancer tissue arrays were purchase from SuperBioChips Lab (Seoul, Republic of Korea). The tissue array contained 40 tumor specimens, 10 normal tissues adjacent to the cancer from prostate cancer patients, whose clinical data, including age, sex, TNM stage, and Gleason score (GS) were informed by the supplier. The tumor tissues were fixed with formalin, paraffin-embedded, and sectioned by microtome in 4-$\mu$m thickness and put on Superfrost plus slides (Gyeonggi, Republic of Korea)

### Plasmids, small interfering RNAs, and transfection

For transient transfection of plasmid or siRNAs, cells were transfected using Lipofectamine 2000 (for plasmid, Thermo Fisher Scientific, Waltham, MA, USA) or Lipofectamine RNAiMAX (for siRNA, Thermo Fisher Scientific), respectively. The transfected cells were stabilized for 48 h before being used in experiments.

The empty vector and *pcDNA3.1-ZBTB16* plasmids were kindly given by prof. KC Jung (Seoul national university). For overexpression of gene, cells were transfected with the following constructs: *pcDNA3.1*-vecter (control), *pcDNA3.1-ZBTB16*, *pCMV*-vector (control), *pCMV*-constitutively activated *STAT3* (*CA-STAT3*).

AllStars Negative Control *siRNA* (Qiagen, Germantown, MD, USA) used as a non-targeting RNAs (*si*CTL). siRNAs for *ZBTB16* (SI00083608, SI00083615, SI03090346), *PTPN6* (SI04436831, SI04950407), *CCL3* (SI03073028, SI03107111), *PLAUR* (SI03033289, SI03048458) were purchased from Qiagen (Germantown, MD, USA). *CCL4* (6351-1, 6351-2), *SERPINE1* (5054-1, 5054-2) were purchased from BIONEER (Daejeon, Republic of Korea).

## Western blot analysis

Cell lysates were prepared using Triton X-100 lysis buffer (150 nM NaCl, 20 mM Tris, 1% Triton X-100, 1% sodium deoxycholate, 0.1% sodium dodecyl sulphate (SDS), 10 mM ethylenediaminetetraacetic acid; EDTA) with protease inhibitors (NaF, $Na_3VO_4$, Leupeptin) and phenylmethanesulfonyl fluoride (PMSF). Lysates were separated via SDS-polyacrylamide gel electrophoresis and then transferred to nitrocellulose membranes (GE Healthcare, Pittsburgh, PA, USA). Membranes were incubated with blocking buffer (TBS with 5%

skimmed milk and 0.1% tween 20) for 1 h at room temperature followed by incubating at 4℃ overnight with tris-buffered saline and tween (TBST) and then incubated with secondary antibody in 1:10000 dilution (Enzo Life Science, Farmingdale, NY, USA) for 1 h at room temperature. The signal was visualized using the ECL detection kit (SurModics, Eden Prairie, MN, USA). With appropriate calculations, sample signals can be accurately normalized to housekeeping proteins designated as internal loading controls to obtain quantitative western blot analysis.

Primary antibodies against PLZF, HDAC1, Fibronectin, N-cadherin (AbCam), SHP-1, Lamin B, PCNA, cyclin D3, CDK4, p21, p27, E-cadherin, PTPN2 (Santa Cruz, CA, USA), Vimentin (R&D systems, Minneapolis, MN, USA) and c-Myc, cyclin D1, BCL-2, BCL-xL, SHP-2, phospho-STAT1 (Tyr701/Ser727), STAT1, phospho-STAT3 (Tyr705/Ser727), STAT3, phospho-STAT5 (Tyr694), STAT5, phospho-JAK1 (Tyr1022/1023), JAK1, phospho-JAK2 (Tyr1007/1008), JAK2, phospho-JAK3 (Tyr980/981), JAK3, phospho-TYK2 (Tyr1054/1055), TYK2 (Cell Signaling Technology) were all diluted to 1:1000. GAPDH (Cell Signaling Technology) antibody was used as loading control.

### RNA extraction, reverse transcription, and quantitative reverse transcription polymerase chain reaction (qRT-PCR) analysis

Total RNA was isolated from cell line using RNAiso Plus reagent

(Takara, Shiga, Japan) according to the manufacturer's instructions. cDNA was synthesized using the ReverTra Ace qPCR RT Master Mix (Toyobo, Osaka, Japan). The gene expression levels were detected by using EvaGreen qPCR Mastermix (Applied Biological Materials, Richmond, Canada) and performed real-time PCR on the Applied Biosystems 7300 Real-time PCR system (Life Technologies) with the following PCR conditions; 95℃ for 2 min, followed by 40 cycles of 95℃ for 15 sec and 60℃ for 1 min. Data were normalized to internal control *GAPDH*.

Primers for *ZBTB16* (QT00029960), *PTPN6* (QT00011725), *STAT3* (QT00068754), *CDH1* (QT00080143), *CDH2* (QT00063196), *VIM* (QT00095794), *FN1* (QT00038024), *CCL3* (QT01008063), *CCL4* (QT01008070), *SERPINE1* (QT00062496), *PLAUR* (QT00076447), *MYC* (QT00035406), *CCND1* (QT00495285), *BCL2* (QT00025011), *BCL2L1* (QT00236712), *MMP9* (QT00040040), *MMP11* (QT00024031), *PTPN2* (QT00020720) and *GAPDH* (QT01658692) were purchased from Qiagen (Germantown, MD, USA).

## Cell proliferation assay

Cell counting kit (CCK) (Dongin-LS, Gyeonggi, Republic of Korea) was performed to detect the cell proliferation capacity. DU145 cells were plated at a density of $5 \times 10^5$ cells per well of a 6-well plate. ; LNCaP cells were plated at a density of $1 \times 10^6$ cells per well of a

6-well plate. For CCK assay, cells were given 24 h to attach and were transfected plasmid and siRNA 24, 48, 72 h. After transfection, cells were incubated with 100 μL/well of the CCK reagent for 2 h at 37℃ and were measured the absorbance of the plates at 450 nm. All values were normalized to the vehicle control-treated wells.

### Apoptosis and cell cycle determination

For cell apoptosis assay, cells were stained with FITC Annexin-V and propidium iodide (PI) kit (Becton Dickinson Bioscience, San Jose, CA, USA) according to the manufacturer's protocol. For cell cycle assay, cells were fixed in cold 70% ethanol and then stained with propidium iodide (Becton Dickinson Bioscience). Cells were then washed with PBS, resuspended in FACS buffer (Becton Dickinson Bioscience), and stained cells were analyzed using FACS LSRFortessa.

### Wound healing assay

Cell migration was assessed by wound healing assay. In brief, cells ($1 \times 10^6$ DU145 cells) in 6-well plates were allowed to reach confluence, and wounds were scratched using sterile tips. Wound closure was monitored every 24 h using a microscope and evaluated wound distances (100×, Nikon, Tokyo, Japan). The experiments were performed in triplication.

## Cell migration and invasion assays

Transwell assay was used to evaluate the migration and invasion abilities of the prostate cancer cells. 24-well transwell chambers with 8 μm pore size polycarbonate membrane (Corning Inc., Corning, NY, USA) were used in these assays. For the transwell assays, the PLZF expression vector and PLZF siRNA were transfected into DU145 or LNCaP cells and resuspended at a concentration of $5 \times 10^4$ cells in the top well with 200 μL serum-free RPMI 1640 media. The lower chamber was filled with a 700 μL mixture of fresh and CMs (1:1) with 10% fetal bovine serum or neutralizing antibody CCL3 (R&D System) were added as a chemoattractant. For cell migration assay, DU145 or LNCaP cells in a serum-free media were seeded into the top chamber and incubated at 37℃ for 24 h. For cell invasion assay, the membrane was coated with Matrigel (Corning Inc.) and incubated at 37℃ for 36 h. Cells on the top surface of the interface membrane were removed using a cotton swab. Migrated and invaded cells on the lower surface of the membrane were fixed with 10% formaldehyde, stained with hematoxylin and eosin kit (Sysmex Corporation, Kobe, Japan), and counted under an optical microscope (100×, Japan) from four random fields using ImageJ software.

## Luciferase gene report assay

For the PLZF target reporter assay, DU145 and LNCaP cells were transiently co-transfected with 1 μg of the *pGL3-PTPN6*

promoter-luciferase reporter construct, *pcDNA3.1-ZBTB16* or *si-ZBTB16*, and *pCMV-β*-galactosidase. After 48 h, cells were lysed and luciferase activity was determined using Luciferase reporter assay system (Promega, Madison, Wisconsin, USA). β-galactosidase activity in each lysate was assayed to normalize transfection efficiency. Three independent experiments were performed with triplicate samples.

### Human proteome profiler cytokine arrays

Human cytokine array kits were used according to the manufacturer's protocol (R&D System). Although membranes were blocked for 1 h, culture supernatants from HDF cells were added to the membranes and incubated with cytokine arrays membranes overnight at 4℃. Membranes were washed and incubated with detection biotinylated antibody cocktail (1:50) at room temperature for 1 h and incubated with horseradish-peroxidase-conjugated streptavidin (1:2000) at room temperature for 30 min, developed using chemi-luminescence-type solution, and exposed to x-ray film. Spot intensities were analyzed using Adobe Photoshop.

### Microscopy, image capture, and analysis

Samples were visualized and analyzed using Leica Aperio AT Turbo microscope and Leopard program included with the microscope

(BX53; Olympus, Tokyo, Japan), using the Leica Application Suite software. Brightness and contrast were adjusted equally in all images presented.

## Statistical analysis

All data were performed with Microsoft Excel 2016 or GraphPad Prism 8 analytical tools (GraphPad software, Inc.), and results were presented as the means ± standard deviation (S.D.) from independently at least three times. Unpaired Student's two-tailed *t*-test for independent analysis was applied to evaluate the differences. The Pearson's correlation was used to evaluate the correlation between PLZF, pY-STAT3, and SHP-1 protein expression. Survival rate analyses were performed by drawing curves and calculating log-rank *P* test using the Kaplan-Meier method. For gene expression and patient survival analyses, I used all available genes in the analysis and divided prostate cancer patients into two classes based on the median expression. Patients were divided into high and low groups according to the 50% cutoff point of gene expression. In prostate cancer, patients with a median or higher scores (≥ 50%) were classified as high-expressing group, and those with less than the median scores (< 50%) were classified as low-expressing group.

# RESULTS

## PLZF inhibits the activation of STAT3 which has an inverse correlation with PLZF

I first evaluated the protein levels of PLZF and Tyr705 phosphorylation of STAT3 (pY-STAT3) in 40 prostate cancer patients and 10 benign patient tissues, which were categorized according to GS. IHC assays showed that the levels of pY-STAT3 increased with the progression of prostate cancer, as opposed to the decrease in PLZF levels (Figure 1A and B). Pearson's correlation analyses revealed a significant negative correlation between PLZF and pY-STAT3 levels (Figure 1C). The Prostate Specific Antigen (PSA) from prostate cancer patients also has been shown to increase with GS (Figure 2A). The pY-STAT3 protein levels are correlated, but the PLZF protein levels are inversely correlated with PSA (Figure 2B). Moreover, prostate cancer patients from The Cancer Genome Atlas (TCGA) database were divided into PLZF- and pY-STAT3-low/high groups. Kaplan-Meier analysis indicated that patients with PLZF-low and pY-STAT3-high groups had poorer recurrence-free survival than those with PLZF-high and pY-STAT3-low expression (Figure 3A). In addition, the PLZF-high group also showed higher survival rates than the PLZF-low groups in the CRPC patient group with the poorest prediction for prostate

cancer (Figure 3B).

Prostate cancer progression is highly dependent on androgen receptor (AR) in the early stage of the disease, and therefore responds well to androgen deprivation therapy (ADT). Adaptation of tumor cells to androgen-low environment has result in AR-sensitive CRPC, a uniformly lethal disease. AR in prostate tumors is expressed in prostate cancer even after androgen blockade, and as *AR* mRNA increases, the sensitivity is very high even in the presence of a small amount of testosterone, so it is easy to combine with other testosterone derivatives, including testosterone secreted by the adrenal glands. PLZF expression was increased in the ventral prostate of castrated mice after androgen replacement [36]. This was further validated in AR positive PCa cell lines LNCaP, VCaP and 22Rv1 [36]. Consistent with this, PLZF expression was undetectable in AR-deficient prostate cancer cell lines DU145 and PC3 and ectopic expression of AR restored PLZF expression in DU145 cells, confirming androgen regulation of rapid and transient expression [37]. These results demonstrate that PLZF is an androgen-activating gene [38]. Therefore, survival was confirmed after dividing the prostate cancer patients with AR-high/low cases except for CRPC into groups with high and low PLZF expression, respectively. As a result, in the patient case with high AR, the lower the PLZF, the worse the prognosis, but it was no significant in the patient case with low AR (Figure 3C). This means that loss of PLZF in prostate cancer is an important target for progression to CRPC and

development of resistance to ADT. Survival curves are divided into two groups based on median scores of the expression.

It was also confirmed that knockdown of PLZF increased the phosphorylation of STAT3 (Figure 4). The mRNA levels of STAT3 were also not significantly changed in PLZF-overexpressed cells (Figure 5A). Besides, pY-STAT3 and total STAT3 proteins did not bind with PLZF (Figure 5B). If only tyrosine, not serine, was reduced by PLZF during phosphorylation of STAT3, the status of the phosphorylation would be questioned when phosphorylated STAT3 was translocated into the nucleus. I performed cytosol-nuclear fractionation with PLZF-overexpressed DU145 cells. The nuclear and cytoplasmic proteins were dissociated, and the Western blot showed that exogenous overexpression of PLZF significantly decreased only tyrosine phosphorylation of STAT3, not serine phosphorylation of STAT3 in both the cytosol and nucleus compared to the control (Figure 6). Reducing pY-STAT3, a well-known oncogene in prostate cancer, suggests that PLZF is likely involved in progression of prostate cancer. Therefore, I hypothesized that PLZF acts as the tumor-suppressor gene to improve the poor prognosis in prostate cancer patients.

## PLZF induces the cell cycle arrest and apoptosis effects by suppression of STAT3 signaling

To investigate the tumor-suppressing role of PLZF in prostate

cancer, I overexpressed PLZF in DU145 cells. Overexpression of PLZF resulted in significantly reduced proliferating cell nuclear antigen (PCNA) protein expression, and inhibited cell growth. In contrast, knockdown of endogenous PLZF increased cell viability in LNCaP cells (Figure 7A–C).

Moreover, to explain that PLZF functions as a tumor suppressor, cell cycle distribution was detected. Cell cycle examined by flow cytometry analysis revealed that 10.83% more cells increased in the sub–G1 phase proportion and 14.75% more cells accumulated in the G0/G1 phase compartment with PLZF–overexpressed DU145 cells ($n$ = 3) (Figure 8A). To confirm the molecular mechanism of PLZF, the expression levels of the cell cycle arrest regulators, including c–MYC, cyclin D1, cyclin D3, CDK4, p21, and p27, were tested. As a result, the G0/G1 phase arrest is confirmed by PLZF (Figure 8B and C). In addition to promoting cell cycle arrest, PLZF triggered prostate cancer cell apoptosis, with effectively increasing the apoptosis proportion in the Annexin V/PI staining assay. Compared to the controls, an increase in the percentage of early and late apoptotic cells was observed in PLZF–overexpressed DU145 (early, from 7.43% to 14.83%; late, from 3.47% to 10.69%; Figure 9A). The mRNA/protein levels of the B–cell lymphoma–extra large 2 (BCL–2) family apoptotic markers were inhibited in PLZF–overexpressed cells, but they were increased in PLZF–knockdown cells (Figure 9B and C). As a result, these findings indicated that the increase in PLZF expression in prostate cancer cells induced cell cycle arrest and

apoptosis.

## PLZF ablation in prostate cancer promotes cell migration and invasion via activation of STAT3

I next evaluated the migration and invasion ability by wound healing assays, transwell cell migration assays, and matrigel invasion assays. Quantitative analysis of the wound healing assay revealed that PLZF-transfected cells delayed the closure of the wound gap as well as delayed the STAT3-knockdown in DU145 cells. (Figure 10A-C). Consistently, a similar effect of PLZF was observed in the transwell cell migration assays. As with the *siSTAT3*-transfected cells, the number of migrated cells with ectopically expressed PLZF showed an apparent reduction compared to the control cells. In contrast, knockdown of endogenous PLZF in LNCaP cells by siRNA increased the cell migration ability. The matrigel invasion assays demonstrated that the cell invasion ability is significantly attenuated by PLZF-overexpressed DU145 cells but is increased by PLZF-knockdown LNCaP cells (Figure 11A and B). The mRNA/protein levels of the epithelial marker (E-cadherin) were increased in PLZF-overexpressed cells but inhibited in PLZF-knockdown cells. In mesenchymal markers (N-cadherin, Vimentin and Fibronectin), the opposite was observed (Figure 11C and D). Furthermore, consistent with an epithelial-mesenchymal transition (EMT) phenotype, DU145 cells exhibited diminished ECM degradation as evidenced by

decreased levels of *MMP9* and *MMP11* expression (Figure 12). The data presented above suggested PLZF could suppress prostate cancer migratory and invasive abilities by preventing the EMT process.

### Tyrosine phosphatase SHP-1 is a direct target of PLZF and inhibits the tyrosine phosphorylation of JAKs-STAT3 signaling

To interrogate the molecular mechanism of PLZF, which has been demonstrated as a tumor-suppressor gene in human prostate cancer cells, and whether it is associated with the oncogenes JAK1, JAK2, and JAK3 as well as the TYK2 (JAKs)-STAT signaling molecules, I ectopically transfected PLZF in DU145 cells. As a result, PLZF inhibits the phosphorylation of the JAKs-STAT3 signaling pathway molecules but not in STAT1 and STAT5. Especially, tyrosine phosphorylation of the JAKs-STAT3 proteins was inhibited in PLZF-overexpressed DU145 cells. In contrast, serine phosphorylation and the total JAKs-STAT proteins remained unchanged (Figure 13). Since PLZF suppresses tyrosine phosphorylation only, it is assumed that PLZF can dephosphorylate JAKs-STAT3 through tyrosine phosphatase. To identify the tyrosine phosphatases related to STAT3, the mRNA/protein levels of protein tyrosine phosphatase SHP-1 were increased in PLZF-overexpressed cells, but they were inhibited in PLZF-knockdown cells (Figure 14A and B). PLZF overexpression significantly induced SHP-1 expression, whereas tyrosine-phosphorylation of JAKs-

STAT3 was abolished by ectopic-PLZF despite SHP-1 ablation (Figure 15).

To determine whether the SHP-1 promoter region contributes to transcriptional regulation of the *ZBTB16* gene, I constructed a *pGL3*-luciferase reporter plasmid containing the SHP-1 promoter fragment. In prostate cancer cell lines, SHP-1 promoter activity was increased by PLZF overexpression, while the activity was diminished by PLZF knockdown (Figure 16). The IHC quantification of SHP-1 protein expression demonstrated that the protein levels are lower in high GS (Figure 17A and B). Pearson's correlation analyses revealed a prominently positive correlation between SHP-1 and PLZF levels (Figure 17C). The SHP-1 protein levels of prostate cancer patient tissues are inversely correlated in PSA (Figure 17D). Moreover, prostate cancer patients from the TCGA database were divided into the SHP-1 high ($n$ = 71)/low ($n$ = 70) expression groups. Kaplan-Meier analysis indicated that patients of low SHP-1 levels had poorer recurrence-free survival than those with high SHP-1 levels. Survival curves are divided into two groups based on median scores of the expression (Figure 17E). These results indicate that PLZF suppressed the tyrosine phosphorylation of JAKs-STAT3 by promoting SHP-1 transcription, acting as a tumor-suppressor gene.

**PLZF is reduced in prostate cancer due to the fibroblast-cancer cell**

interaction.

Fibroblasts are one of the most abundant cell types in the prostate stroma. Fibroblasts synthesize many components of ECM (collagens I, II, and V, and fibronectin) and are responsible for the remodeling of ECM by secreting matrix metalloproteinases (MMPs). Fibroblasts also secrete growth factors and cytokines to regulate differentiation and homeostasis of adjacent epithelium. In some physiological (inflammation) or pathological (cancer) conditions, fibroblasts have an activated phenotype due to stimulation by growth factors or cytokines [39]. In prostate cancer progressions, interactions with various tumor microenvironment cells, including cancer cells and fibroblasts, are known to play an important role [8,11,12]. In this study, I hypothesized that fibroblasts interacting with cancer cells suppress PLZF expression and enhance malignant behaviors. To examine the cells affecting cancer cells among various stromal cells in the tumor microenvironment, LNCaP cells were co-cultured with Jurkat-T, NK-92, THP-1 and fibroblasts. Interestingly, only the LNCaP sample co-cultured with the fibroblast suppressed PLZF levels (Figure 18).

To determine the influence of fibroblasts on prostate cancer, I adopted a co-culturing system using transwell chambers (Figure 19). Surprisingly, I found that both protein and RNA expression of PLZF were more reduced by direct co-culturing of fibroblast and cancer cells than fibroblast CM (FCM). The direct co-culturing systems enable the sharing of media and soluble factors throughout the entire

culture well. These results indicated that co-culturing with fibroblast was expected to promote the malignancy of prostate cancer cells (Figure 20A). In addition, both protein and RNA expression of PLZF were confirmed with the same results in PLZF-overexpressed DU145 cells as in LNCaP cells (Figure 20B). These results indicated that co-culturing with fibroblast was expected to promote the malignancy of prostate cancer cells. To understand the functional role of FCM and direct co-culturing in prostate cancer, I examined cell proliferation, migration, and invasion assays. LNCaP cells proliferation was further increased by the co-cultured CM (Co-CM) than FCM through the CCK assay (Figure 21). Next, transwell cell migration and matrigel invasion assays were examined, and Co-CM significantly promoted cell migration and invasion in LNCaP cells rather than FCM (Figure 22A). The mRNA/protein levels of the mesenchymal markers were more increased in the LNCaP cells treated with Co-CM, whereas E-cadherin was more decreased than FCM (Figure 22B and C). To confirm that normal fibroblasts increased the malignancies of cancer cells, non-normal cells, the normal prostatic epithelial cell line (PNT2), and LNCaP cells were co-cultured with fibroblasts. In PLZF-overexpressed PNT2 cells, the PLZF levels were not significantly affected by co-culturing with fibroblasts; however, PLZF levels were substantially inhibited by co-culturing with fibroblasts in LNCaP cells (Figure 23). Taken together, these findings further support the functional significance of fibroblasts in the tumor microenvironment, in that they remarkably promote the malignant behavior of prostate cancer cells.

**Loss of CCL3 inhibits the fibroblast-induced prostate cancer cells migration and invasion.**

To confirm whether the fibroblast-derived factors in CM is a polypeptide, Co-CM was treated or heated with mixture of CM and fresh media. Consequently, the fibroblast-inducing effect was practically abolished by heat inactivation (Figure 24).

To explore the soluble mediators released by the fibroblast and fibroblast co-cultured with prostate cancer cells, I analyzed by using protein arrays the levels of multiple cytokines, chemokines, and growth factors (Figure 25A and B). These candidates that were more enriched in co-cultured CM (Co-CM) than prostate cancer cell CM (CTL CM) and fibroblast CM (FCM) were identified: CCL3/4, SERPINE1, and urokinase-type plasminogen activator receptor (uPAR, *PLAUR*). To evaluate the increase in the identified cytokines, fibroblasts were co-cultured with the normal prostate cells (PNT2) or the prostate cancer cells (LNCaP, DU145). In contrast to no effect on *CCL4* and *SERPINE1* mRNA expression, mRNA expression of *CCL3* and *PLAUR* was visibly induced in co-culture between prostate cancer cells and fibroblast. In other words, cancer cells and fibroblasts contribute to maligning tumors by affecting each other (Figure 26). To determine the cytokine responsible for PLZF suppression, each of the four candidates was knocked down in fibroblast and cancer cells using siRNAs. Knockdown of *CCL3* or *PLAUR*, but not *CCL4* or *SERPINE1*, attenuated the PLZF protein expression suppression by Co-CM (Figure 27A and B). To confirm

the PLZF-suppressing effects of the two cytokines (CCL3, uPAR), neutralizing antibodies were administered to FCM and Co-CM. Only anti-CCL3 Abs alone abolished the PLZF-inhibitory effect (Figure 27C). In this study, PLZF acts as a transcription factor of the SHP-1 gene. Therefore, to investigate whether CCL3 inhibits PLZF-mediated transcription of the SHP-1 gene, prostate cancer cells were treated with a recombinant CCL3. As a result, SHP-1-driven transcription was more inhibited with Co-CM than FCM by CCL3 (Figure 28A and B). These results suggest that if fibroblasts present near cancer cells, fibroblasts interacting with prostate cancer cells are expected to produce CCL3 more abundantly than normal fibroblast cells. Moreover, by neutralizing CCL3, cell migration and invasion abilities were further abolished by Co-CM, more than FCM (Figure 29A). As a result of the confirmed mRNA/protein levels reinforcing the EMT assays, the alteration in EMT markers expression was abolished by the antibody of CCL3 (Figure 29B and C). Collectively, these results indicate that CCL3 secreted by fibroblasts co-cultured with prostate cancer cells inhibits tumor suppressor PLZF expression in prostate cancer.

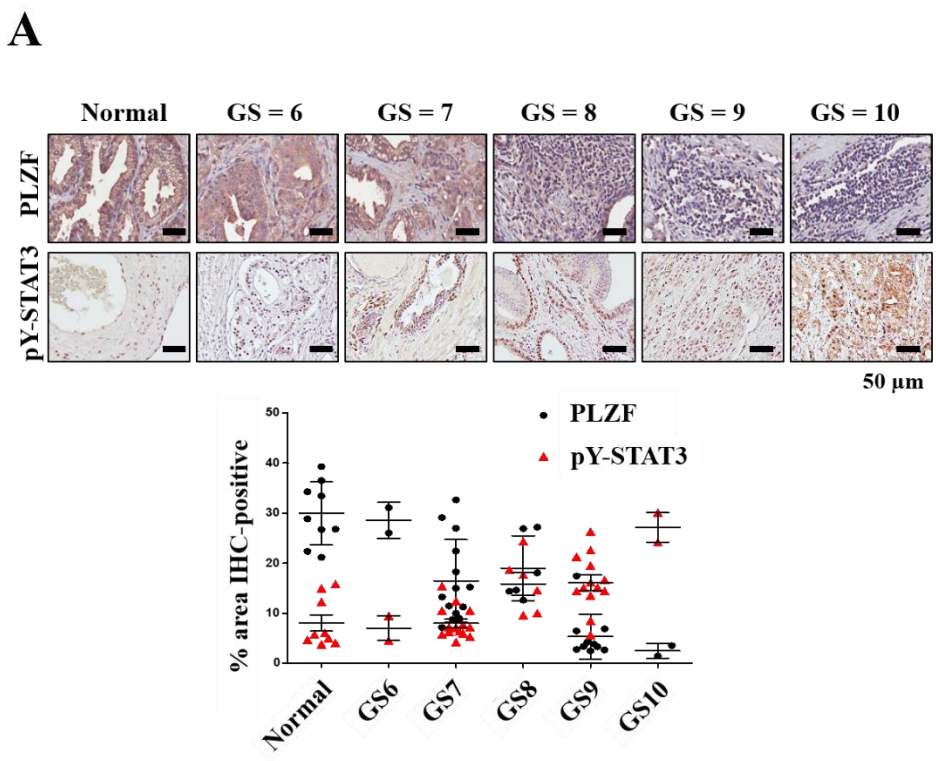
A
Normal
GS = 6
GS = 7
GS = 8
GS = 9
GS = 10
PLZF
pY-STAT3
50 μm
PLZF
pY-STAT3
% area IHC-positive
Normal
GS6
GS7
GS8
GS9
GS10
B
PLZF
pY-STAT3
Normal
Tumor
50 μm
C
pearson r = -0.3593
P = 0.0180
n = 40
pY-STAT3 expression (%)
PLZF expression (%)

**Figure 1. PLZF expression negatively correlates with high-grade prostate cancer patient tissue and STAT3 activation.**

(A) IHC staining (top) of human prostate tissues (normal, cancer) were performed using an anti-PLZF Abs and anti-pY-STAT3 Abs. Quantification of PLZF-positive expression according to the GS in normal tissues adjacent to the benign tumors ($n$ = 9) and malignant tumors ($n$ = 40) (bottom). The images were visualized by Leica Aperio AT Turbo digital pathology scanner (magnification = 400×). (B) Representative IHC staining image of normal prostate and prostate tumor tissues from the same tissue sections. (C) Associations between expression of PLZF and pY-STAT3. Scatter plots showing the linear correlation determined by Pearson correlation coefficient calculation of those genes that were statistically significant. Pearson correlation coefficient $r$ and $P$-values are given in each scatter plot [67].

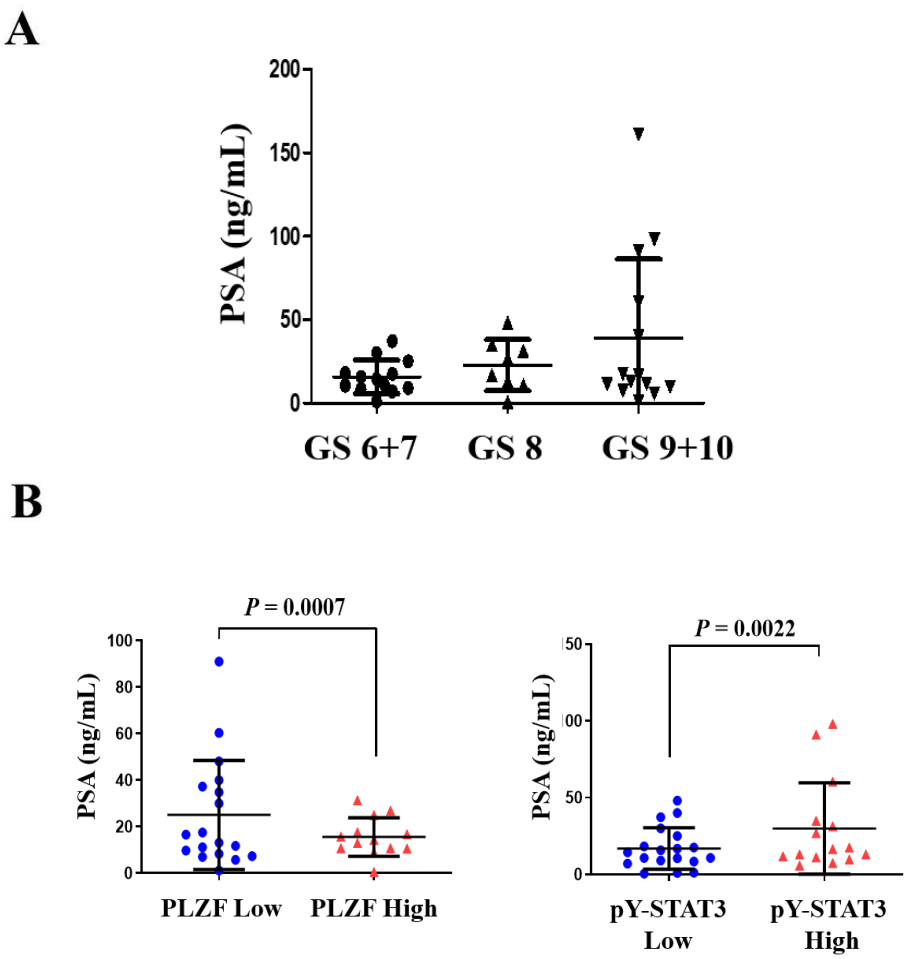


Figure 2. PSA patterns of PLZF and STAT3 activation levels in prostate cancer patient tissues.

(A) PSA levels were measured according to the GS in human prostate cancer specimens, $n$ = 40. (B) PSA levels were measured according to the PLZF ($P$ = 0.0007) and pY-STAT3 ($P$ = 0.0022) protein levels, $n$ = 40 [67].

**A**

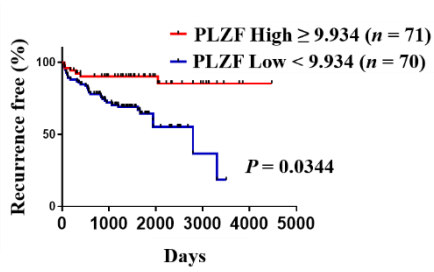
PLZF High ≥ 9.934 (n = 71)
PLZF Low < 9.934 (n = 70)
Recurrence free (%)
100
50
0
P = 0.0344
0 1000 2000 3000 4000 5000
Days

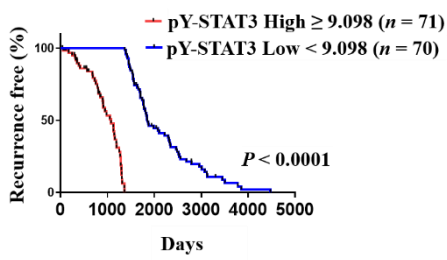
pY-STAT3 High ≥ 9.098 (n = 71)
pY-STAT3 Low < 9.098 (n = 70)
Recurrence free (%)
100
50
0
P < 0.0001
0 1000 2000 3000 4000 5000
Days

**B**

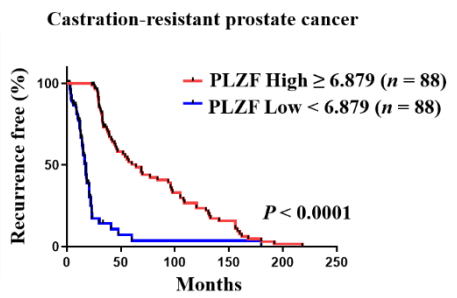
Castration-resistant prostate cancer
PLZF High ≥ 6.879 (n = 88)
PLZF Low < 6.879 (n = 88)
Recurrence free (%)
100
50
0
P < 0.0001
0 50 100 150 200 250
Months

**C**

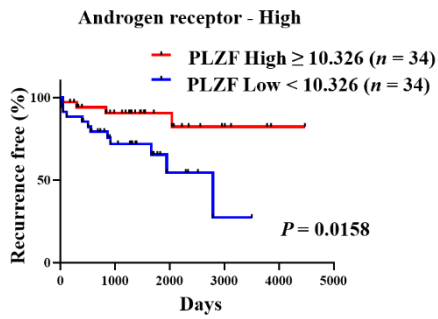
Androgen receptor - High
PLZF High ≥ 10.326 (n = 34)
PLZF Low < 10.326 (n = 34)
Recurrence free (%)
100
50
0
P = 0.0158
0 1000 2000 3000 4000 5000
Days

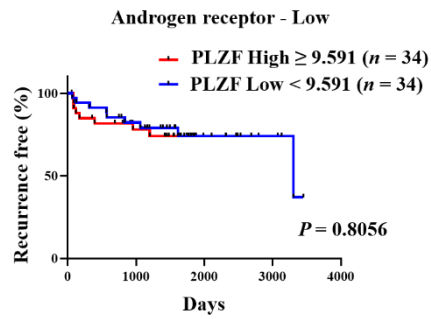
Androgen receptor - Low
PLZF High ≥ 9.591 (n = 34)
PLZF Low < 9.591 (n = 34)
Recurrence free (%)
100
50
0
P = 0.8056
0 1000 2000 3000 4000
Days

**Figure 3. PLZF expression inversely correlates with survival in prostate cancer patients.**

Kaplan–Meier analysis of recurrence–free survival when prostate cancer patients are divided into two groups based on median of the expression scores. Results were analyzed from TCGA database. (A) Kaplan-Meier recurrence–free survival analysis based on median expression scores of PLZF (high ≥ 9.934, low < 9.934, $P = 0.0344$) and pY–STAT3 (high ≥ 9.098, low < 9.098, $P < 0.0001$). (B) Kaplan–Meier recurrence–free survival analysis of CRPC patients based on median expression scores of PLZF (high ≥ 6.879, low < 6.879, $P < 0.0001$) expression. (C) Kaplan–Meier recurrence–free survival analysis of AR–dependent patients based on median expression scores of PLZF expression (AR–high; 10,326; $P = 0.0158$, AR–low; 9.591; $P = 0.8056$) [67].

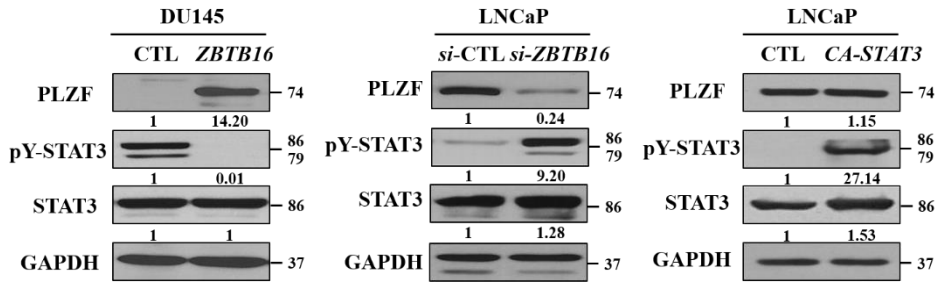


Figure 4. PLZF inhibits tyrosine phosphorylation of STAT3 in prostate cancer cell lines.

DU145 cells were transfected with 2 μg of *pcDNA3.1-ZBTB16* plasmid (left), and transfected cells were incubated for 48 h. LN229 cells were transfected with 50 nM *si-ZBTB16* (middle) or 2 μg of *STAT3* constitutively activated plasmid (right), and transfected cells were incubated for 48 h. The cell lysates were subjected to western blotting. The band intensity of indicated proteins is expressed as a numerical value, relative to GAPDH [67].

**A**

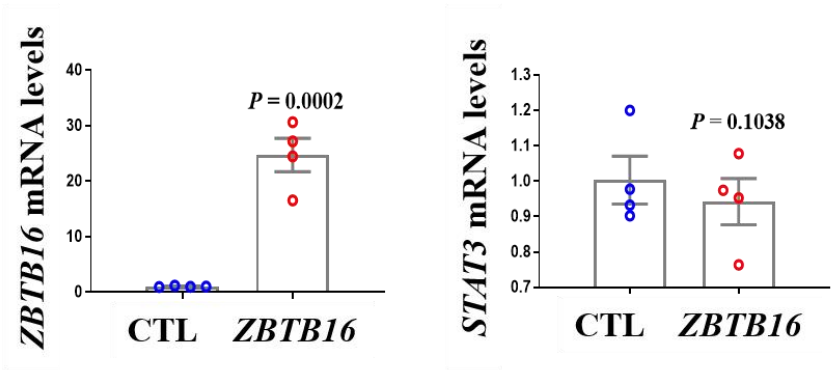
ZBTB16 mRNA levels
P = 0.0002
CTL
ZBTB16
STAT3 mRNA levels
P = 0.1038
CTL
ZBTB16

**B**

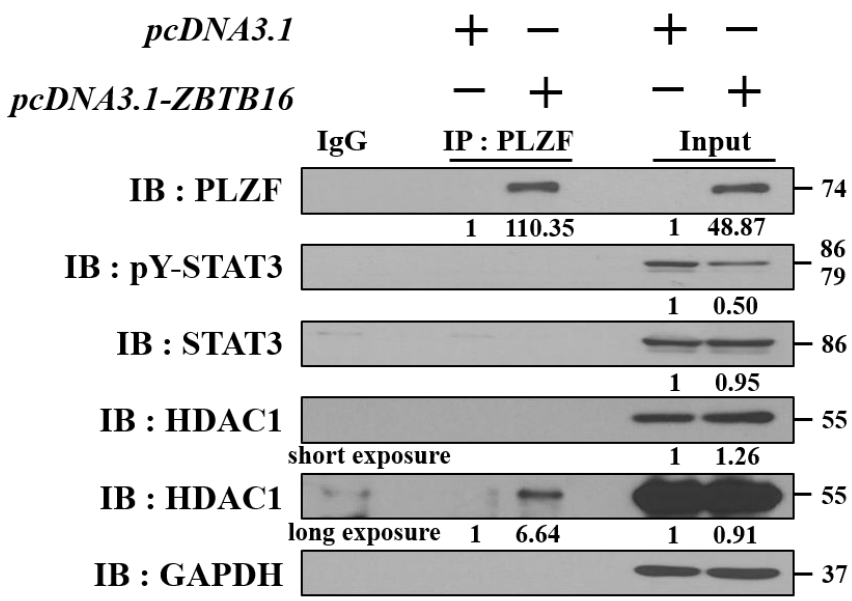
pcDNA3.1
pcDNA3.1-ZBTB16
IgG
IP : PLZF
Input
IB : PLZF
74
1 110.35 1 48.87
IB : pY-STAT3
86
79
1 0.50
IB : STAT3
86
1 0.95
IB : HDAC1
55
short exposure
1 1.26
IB : HDAC1
55
long exposure 1 6.64 1 0.91
IB : GAPDH
37

**Figure 5. PLZF does not affect total STAT3 expression or protein-protein binding with STAT3.**

(A) mRNA expression levels of *ZBTB16*, total *STAT3* were examined by qRT-PCR in DU145 cells transfected with PLZF plasmid. Data represented as the means ± S.D. from 4 independent experiments. (B) Detection of the interaction between PLZF and STAT3 (phosphorylation, total) by co-IP. The protein extract of PLZF was immunoprecipitated by anti-pY-STAT3 Abs and anti-STAT3 Abs. The precipitate was subjected to Western blotting with the antibodies. HDAC1 is a positive control that is well known to form a transcriptional repressor complex with PLZF. The band intensity of indicated proteins is expressed as a numerical value, relative to GAPDH [67].

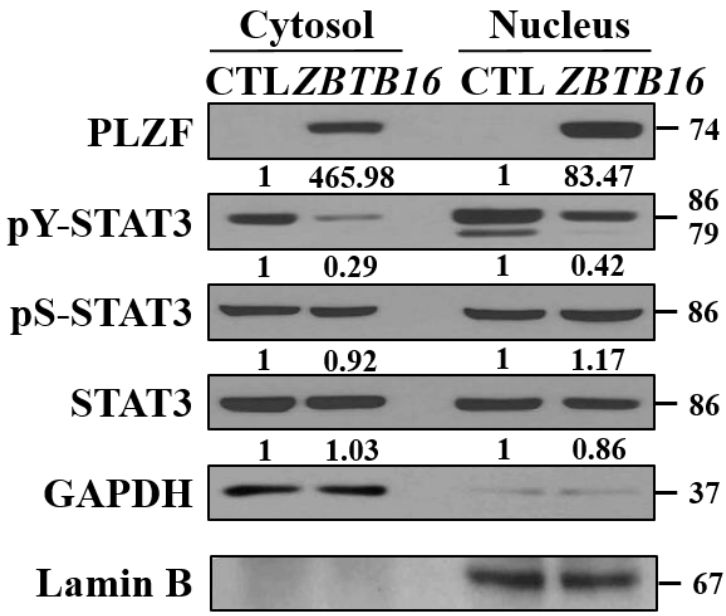


Figure 6. PLZF reduces tyrosine phosphorylation, not serine phosphorylation, of STAT3 in both cytosol and nucleus.

DU145 cells were transfected with 2 ㎍ of *pcDNA3.1-ZBTB16* for 48 h, total lysates were fractionated to cytosolic and nuclear components, which were immunoblotted with the indicated antibodies. The band intensity of indicated proteins is expressed as a numerical value, relative to GAPDH and Lamin B [67].

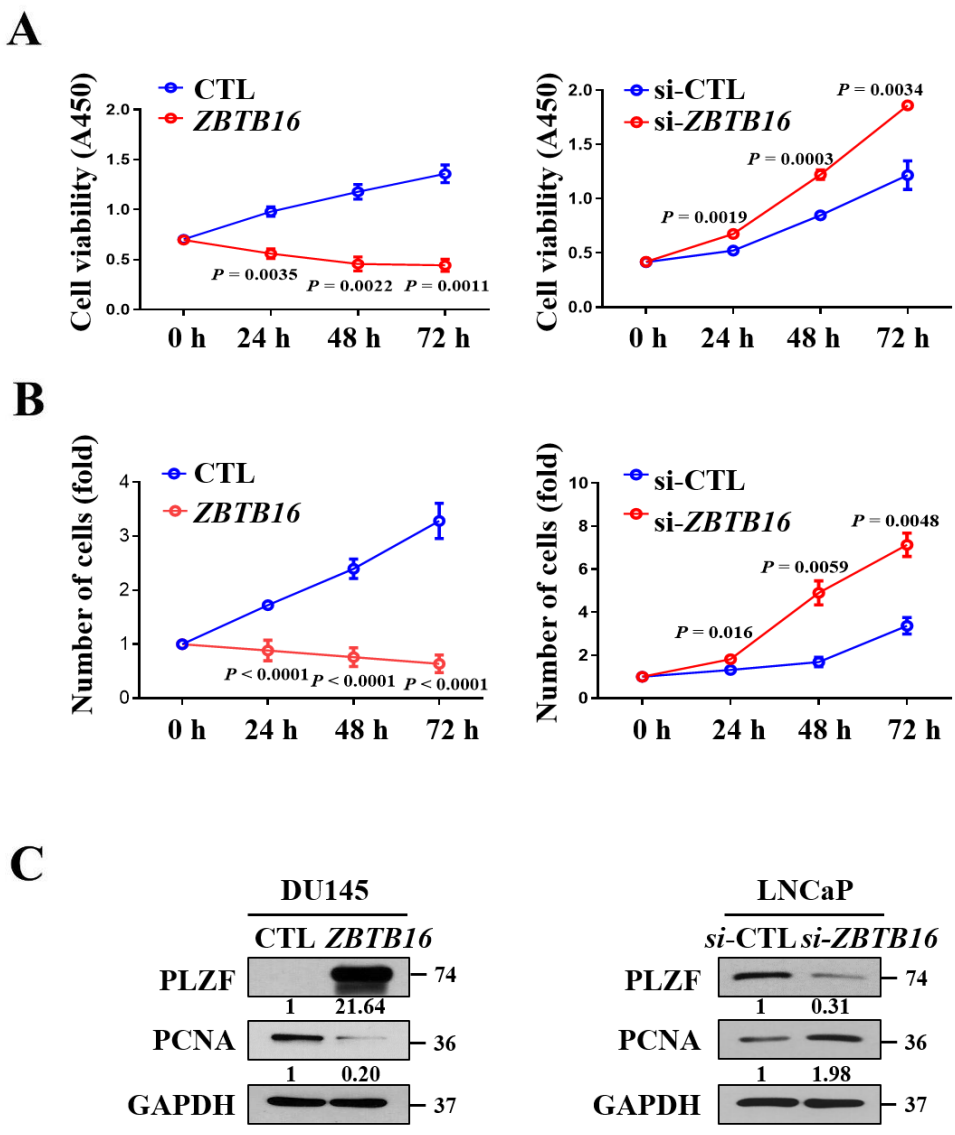
A
CTL
ZBTB16
Cell viability (A450)
2.0
1.5
1.0
0.5
0.0
P = 0.0035
P = 0.0022
P = 0.0011
0 h
24 h
48 h
72 h
si-CTL
si-ZBTB16
P = 0.0034
P = 0.0003
P = 0.0019
B
Number of cells (fold)
4
3
2
1
0
P < 0.0001
P < 0.0001
P < 0.0001
10
8
6
4
2
P = 0.0048
P = 0.0059
P = 0.016
C
DU145
CTL ZBTB16
PLZF
74
1
21.64
PCNA
36
1
0.20
GAPDH
37
LNCaP
si-CTL si-ZBTB16
PLZF
74
1
0.31
PCNA
36
1
1.98
GAPDH
37

Figure 7. PLZF decreases prostate cancer cell viability.

DU145 cells were transfected with 2 ㎍ of *pcDNA3.1-ZBTB16* (left) or LNCaP cells were transfected with 50 nM *si-ZBTB16* (right). (A) CCK assay was performed by transfecting DU145 and LNCaP cells with plasmid and siRNA, respectively, followed by culture for 1-3 days. (B) Cell counting assay was conducted in *ZBTB16* plasmid or *si-ZBTB16*-transfected cells. (C) The transfected cell lysates were subjected to western blotting for proliferation marker. The band intensity of indicated proteins is expressed as a numerical value, relative to GAPDH. Data represented as the means ± S.D. from 3 independent experiments [67].

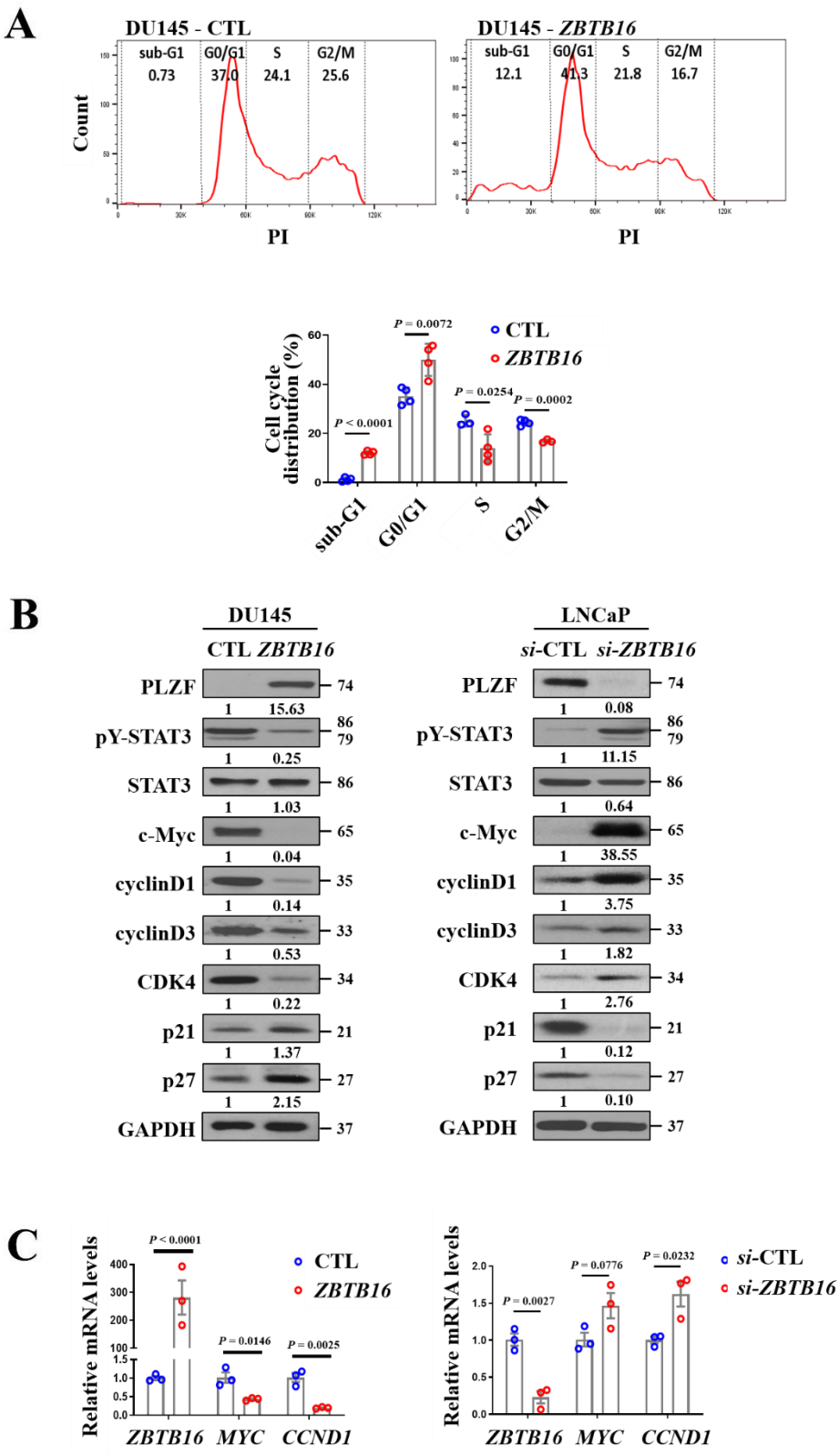
A
DU145 - CTL
sub-G1 0.73
G0/G1 37.0
S 24.1
G2/M 25.6
DU145 - ZBTB16
sub-G1 12.1
G0/G1 41.3
S 21.8
G2/M 16.7
Count
PI
Cell cycle distribution (%)
CTL
ZBTB16
P = 0.0072
P = 0.0254
P = 0.0002
P < 0.0001
sub-G1
G0/G1
S
G2/M
B
DU145
CTL ZBTB16
LNCaP
si-CTL si-ZBTB16
PLZF
pY-STAT3
STAT3
c-Myc
cyclinD1
cyclinD3
CDK4
p21
p27
GAPDH
C
Relative mRNA levels
P < 0.0001
P = 0.0146
P = 0.0025
ZBTB16
MYC
CCND1
si-CTL
si-ZBTB16
P = 0.0027
P = 0.0776
P = 0.0232

**Figure 8. PLZF induces G0/G1 phase arrest in prostate cancer cell lines.**

(A) Effect of cell cycle distribution of CTL- and PLZF-transfected DU145 cells was detected by flow cytometry analysis. Representative histograms of cell cycle alteration (top). Summarized results from four independent experiments were quantified as mean ± S.D. (bottom). (B) Protein expression levels of indicated cell cycle regulators were detected by Western blotting. The band intensity of indicated proteins is expressed as a numerical value, relative to GAPDH. (C) mRNA expression levels of *ZBTB16*, *MYC*, and *CCND1* were examined by qRT-PCR in DU145 and LNCaP cells transfected with *ZBTB16* plasmid and siRNA. Data represented as the means ± S.D. from 3 independent experiments [67].

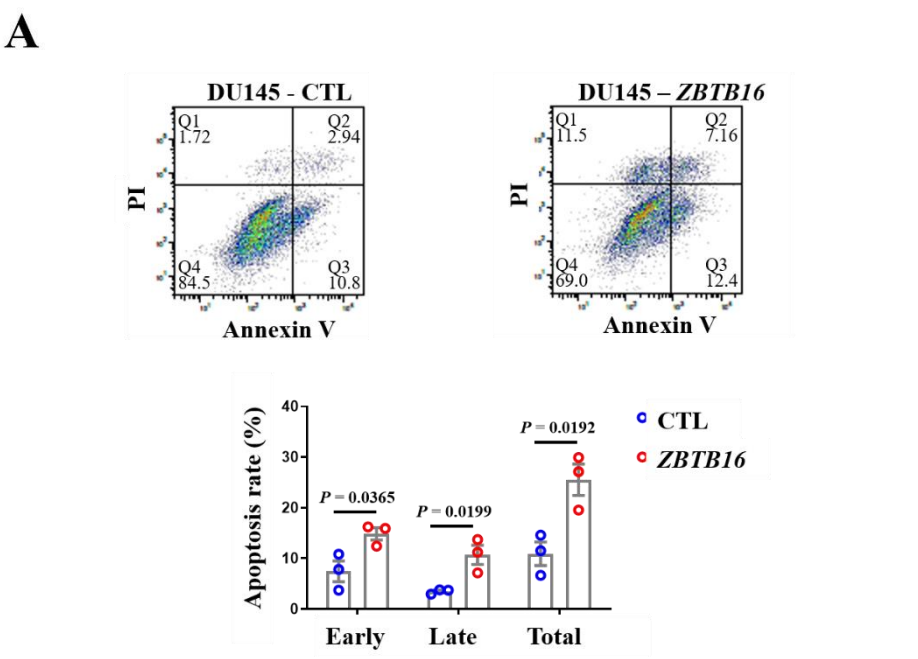
A
DU145 - CTL
Q1 1.72
Q2 2.94
Q4 84.5
Q3 10.8
PI
Annexin V
DU145 – ZBTB16
Q1 11.5
Q2 7.16
Q4 69.0
Q3 12.4
PI
Annexin V
Apoptosis rate (%)
P = 0.0365
P = 0.0199
P = 0.0192
CTL
ZBTB16
Early
Late
Total
B
DU145
CTL ZBTB16
PLZF 74
1 14.24
BCL-2 26
1 0.20
BCL-xL 30
1 0.27
GAPDH 37
LNCaP
si-CTL si-ZBTB16
PLZF 74
1 0.20
BCL-2 26
1 2.06
BCL-xL 30
1 2.16
GAPDH 37
C
Relative mRNA levels
P = 0.1144
P = 0.0044
CTL
ZBTB16
BCL-2
BCL2L1
Relative mRNA levels
P = 0.1053
P < 0.0001
si-CTL
si-ZBTB16
BCL-2
BCL2L1

Figure 9. PLZF induces apoptosis in prostate cancer cell lines.

(A) Apoptosis assay of *pcDNA3.1-ZBTB16* plasmid transfected DU145 cells was detected by Annexin V-FITC/PI staining. The numbers of apoptotic cells are presented as bar graphs. The total bar graph is the sum of the early and late apoptotic values. (B) Protein expression levels of indicated apoptosis regulators were detected by Western blotting. The band intensity of indicated proteins is expressed as a numerical value, relative to GAPDH. (C) mRNA expression levels of *BCL2* and *BCL2L1* were examined by qRT-PCR in DU145 and LNCaP cells transfected with *ZBTB16* plasmid and siRNA, respectively. Data represented as the means ± S.D. from 3 independent experiments [67].

**A**

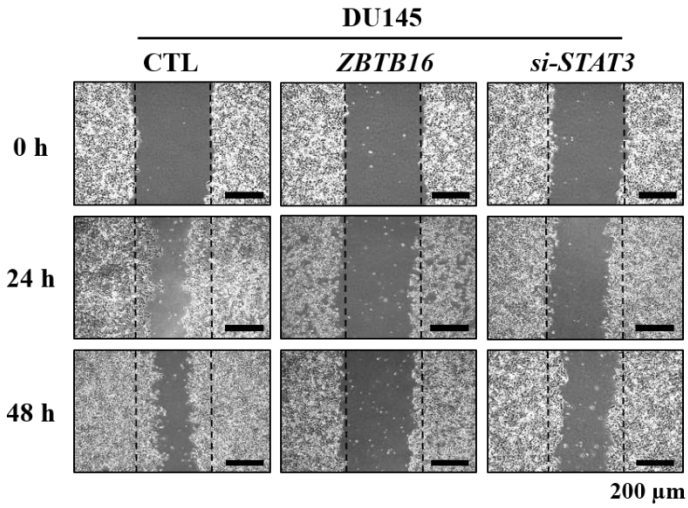
DU145
CTL
ZBTB16
si-STAT3
0 h
24 h
48 h
200 μm

**B**

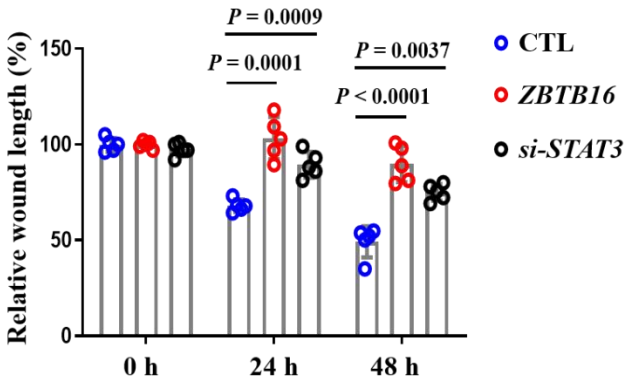
P = 0.0009
P = 0.0001
P = 0.0037
P < 0.0001
Relative wound length (%)
150
100
50
0
0 h
24 h
48 h
CTL
ZBTB16
si-STAT3

**C**

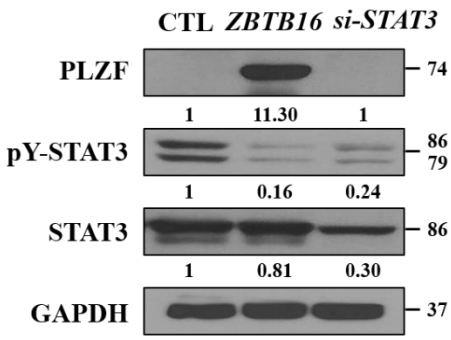
CTL ZBTB16 si-STAT3
PLZF
74
1 11.30 1
pY-STAT3
86
79
1 0.16 0.24
STAT3
86
1 0.81 0.30
GAPDH
37

Figure 10. PLZF and knockdown of STAT3 decrease the migration in DU145 cells.

(A) Wound healing assay of cells from DU145 incubated for 24, 48 h with *pcDNA3.1-ZBTB16* plasmid (2 ㎍) or *si-STAT3* (50 nM). The images were visualized by phase-contrast microscopy (magnification = 100×). (B) The length of wound healing are presented as bar graphs. Data represented as the means ± S.D. from 5 independent experiments. (C) Western blotting was conducted in *pcDNA3.1-ZBTB16* plasmid and *si-STAT3*-transfected DU145 cells. The band intensity of indicated proteins is expressed as a numerical value, relative to GAPDH [67].

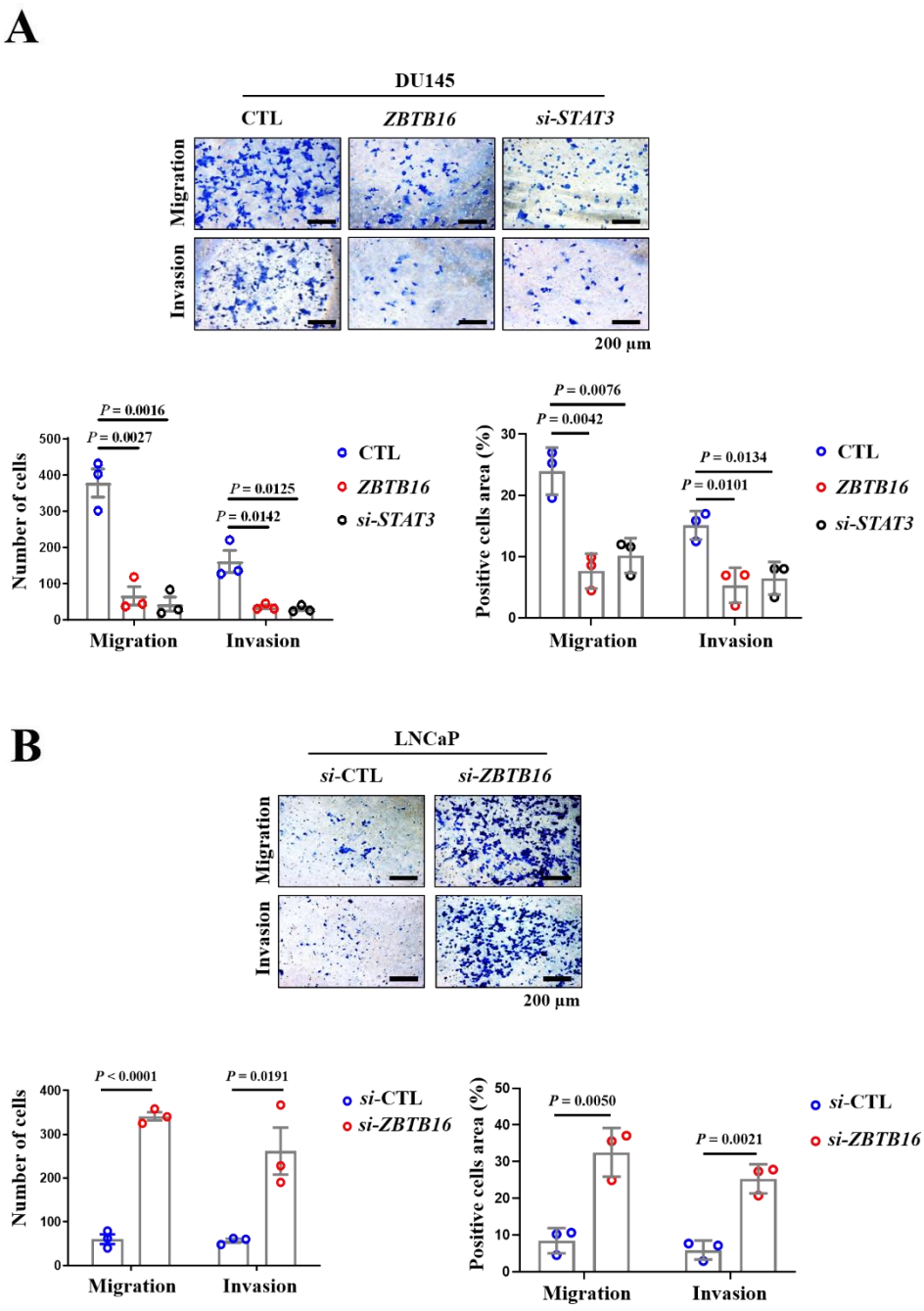
A
DU145
CTL
ZBTB16
si-STAT3
Migration
Invasion
200 μm
Number of cells
P = 0.0016
P = 0.0027
P = 0.0125
P = 0.0142
CTL
ZBTB16
si-STAT3
Migration
Invasion
Positive cells area (%)
P = 0.0076
P = 0.0042
P = 0.0134
P = 0.0101
B
LNCaP
si-CTL
si-ZBTB16
200 μm
P < 0.0001
P = 0.0191
P = 0.0050
P = 0.0021

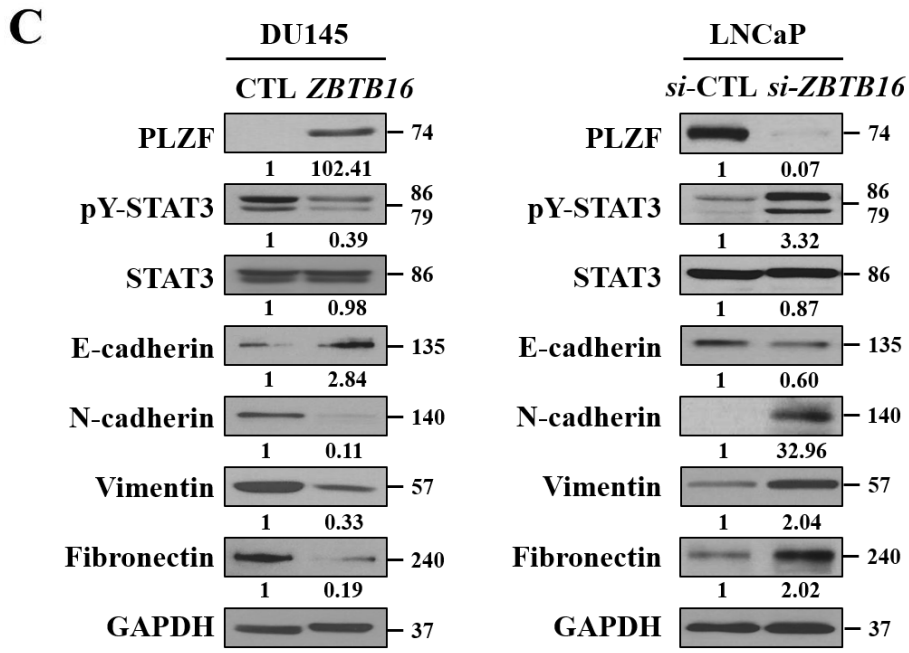
C
DU145
CTL ZBTB16
PLZF
74
1 102.41
pY-STAT3
86
79
1 0.39
STAT3
86
1 0.98
E-cadherin
135
1 2.84
N-cadherin
140
1 0.11
Vimentin
57
1 0.33
Fibronectin
240
1 0.19
GAPDH
37
LNCaP
si-CTL si-ZBTB16
PLZF
74
1 0.07
pY-STAT3
86
79
1 3.32
STAT3
86
1 0.87
E-cadherin
135
1 0.60
N-cadherin
140
1 32.96
Vimentin
57
1 2.04
Fibronectin
240
1 2.02
GAPDH
37

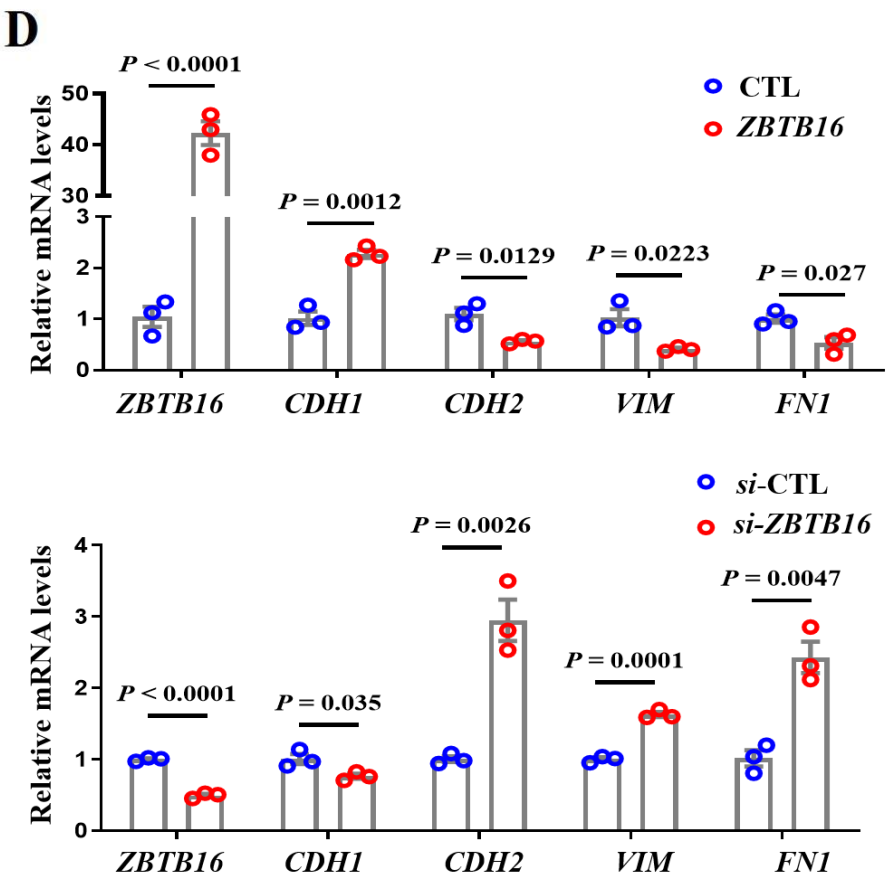
D
Relative mRNA levels
CTL
ZBTB16
P < 0.0001
P = 0.0012
P = 0.0129
P = 0.0223
P = 0.027
ZBTB16
CDH1
CDH2
VIM
FN1
si-CTL
si-ZBTB16
P = 0.0026
P = 0.0047
P = 0.0001
P < 0.0001
P = 0.035

**Figure 11. PLZF reduces the migration and invasion ability in prostate cancer cell lines.**

(A and B) Transwell migration and matrigel invasion assays were conducted in *ZBTB16* or *si-STAT3* and *si-ZBTB16* transfected DU145 and LNCaP cells, respectively. The images (upper) were visualized by phase-contrast microscopy (magnification = 100×). The numbers (bottom, left) or the stained areas (bottom, right) of migrated and invaded cells are presented as bar graphs. (C) DU145 cells were transfected with 2 ㎍ of *pcDNA3.1-ZBTB16* plasmid (left), and transfected cells were incubated for 48 h. LN229 cells were transfected with 50 nM *si-ZBTB16* (right), and transfected cells were incubated for 48 h. The cell lysates were subjected to western blotting for epithelial/mesenchymal related markers. The band intensity of indicated proteins is expressed as a numerical value, relative to GAPDH. (D) mRNA expression levels of epithelial/mesenchymal related markers were examined by qRT-PCR in DU145 and LNCaP cells transfected with *pcDNA3.1-ZBTB16* plasmid and siRNA, respectively. Data represented as the means ± S.D. from 3 independent experiments [67].

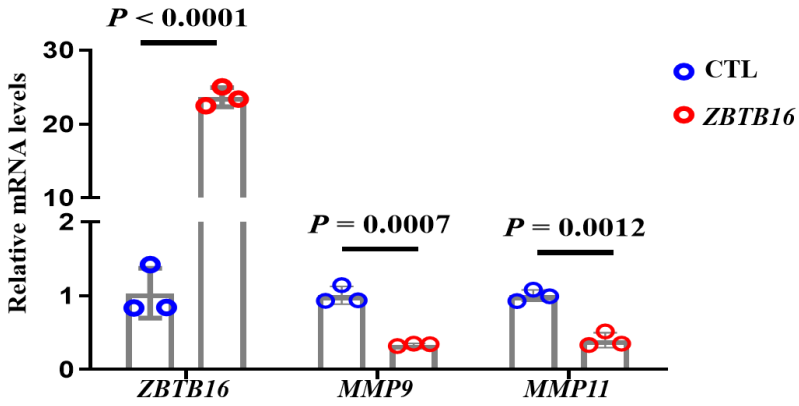


Figure 12. PLZF diminished ECM degradation as evidenced by decreased levels of MMP9 and MMP11.

mRNA expression levels of *ZBTB16, MMP9, MMP11* were examined by qRT-PCR in DU145 cells transfected with *pcDNA3.1-ZBTB16* plasmid. Data represented as the means ± S.D. from 3 independent experiments [67].

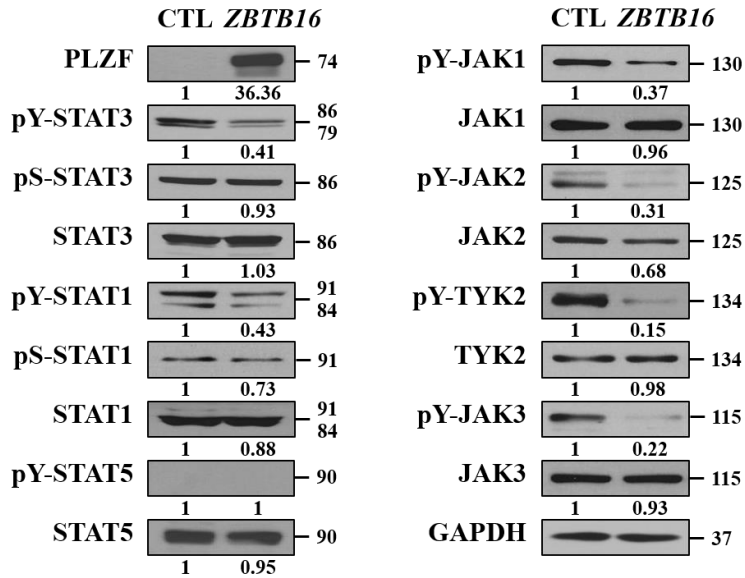


Figure 13. PLZF inhibits the tyrosine phosphorylation of JAKs-STAT signaling.

DU145 cells were transfected with *pcDNA3.1-ZBTB16* plasmid, and then performed western blotting for JAKs-STAT family members. The band intensity of indicated proteins is expressed as a numerical value, relative to GAPDH [67].

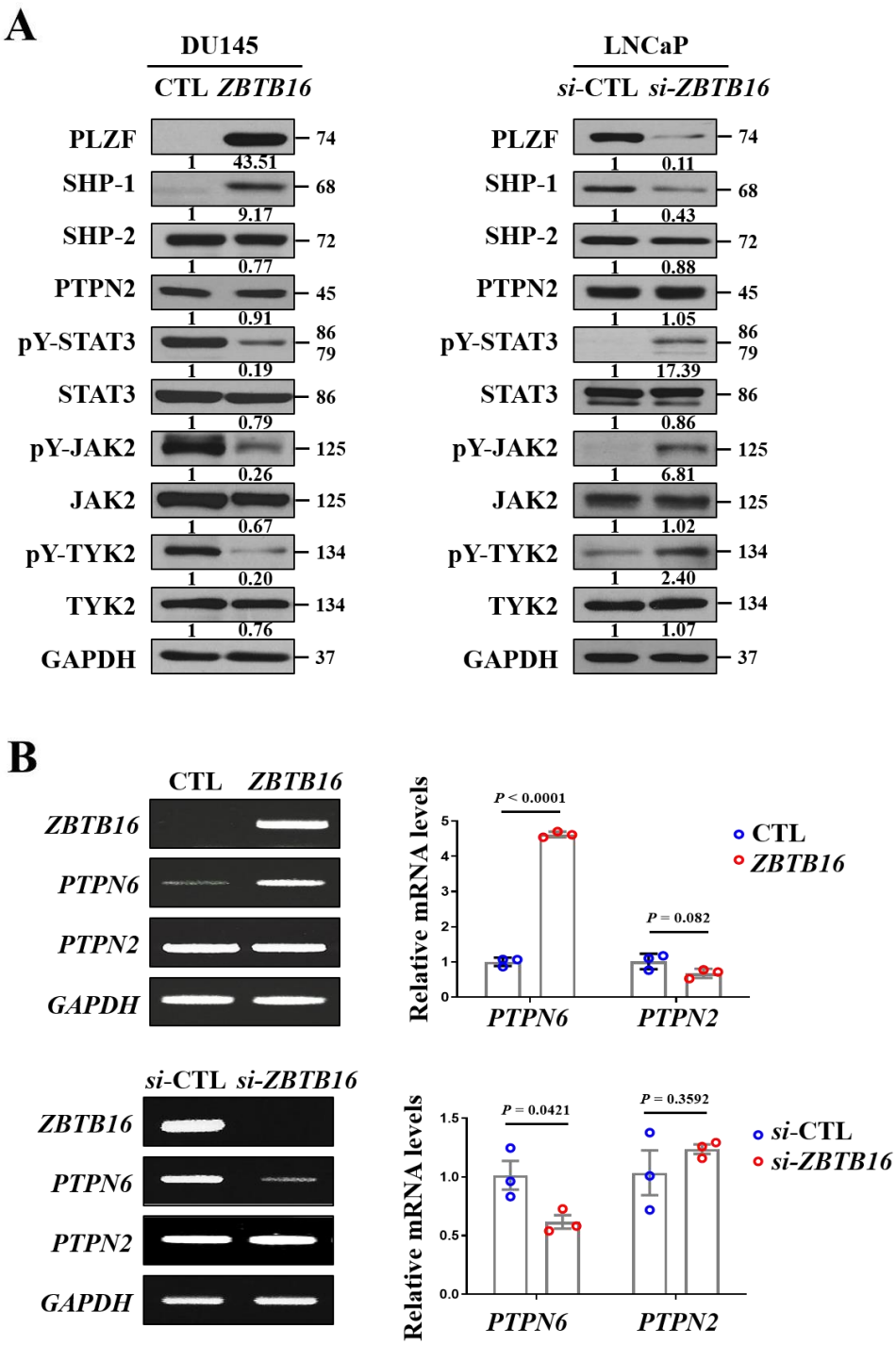
A
DU145
CTL ZBTB16
PLZF
SHP-1
SHP-2
PTPN2
pY-STAT3
STAT3
pY-JAK2
JAK2
pY-TYK2
TYK2
GAPDH
74
68
72
45
86
79
125
134
37
1 43.51
1 9.17
1 0.77
1 0.91
1 0.19
1 0.79
1 0.26
1 0.67
1 0.20
1 0.76
LNCaP
si-CTL si-ZBTB16
1 0.11
1 0.43
1 0.88
1 1.05
1 17.39
1 0.86
1 6.81
1 1.02
1 2.40
1 1.07
B
CTL ZBTB16
ZBTB16
PTPN6
PTPN2
GAPDH
Relative mRNA levels
P < 0.0001
P = 0.082
CTL
ZBTB16
PTPN6
PTPN2
si-CTL si-ZBTB16
P = 0.0421
P = 0.3592
si-CTL
si-ZBTB16

Figure 14. PLZF inhibits the tyrosine phosphorylation of JAKs-STAT3 signaling by increasing SHP-1.

(A) Protein expression levels of the tyrosine phosphatase-related markers STAT3, JAK2, and TYK2 were detected by Western blotting. The band intensity of indicated proteins is expressed as a numerical value, relative to GAPDH. (B) mRNA expression levels of tyrosine phosphatases were examined by RT-PCR (left) and qRT-PCR (right) in DU145 (upper) and LNCaP (bottom) cells. Data represented as the means ± S.D. from 3 independent experiments [67].

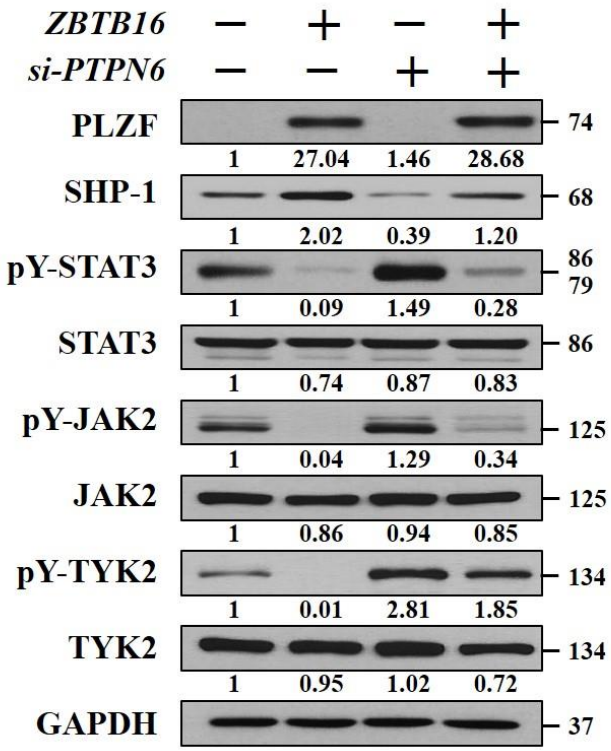


Figure 15. PLZF suppresses tyrosine phosphorylation of JAKs-STAT3 signaling by increasing SHP-1.

LN229 cells were co-transfected with 2 ㎍ of *pcDNA3.1-ZBTB16* plasmid or 50 nM *si-PTPN6*, and transfected cells were incubated for 48 h. The cell lysates were subjected to western blotting for SHP-1, STAT3, JAK2, and TYK2. The band intensity of indicated proteins is expressed as a numerical value, relative to GAPDH [67].

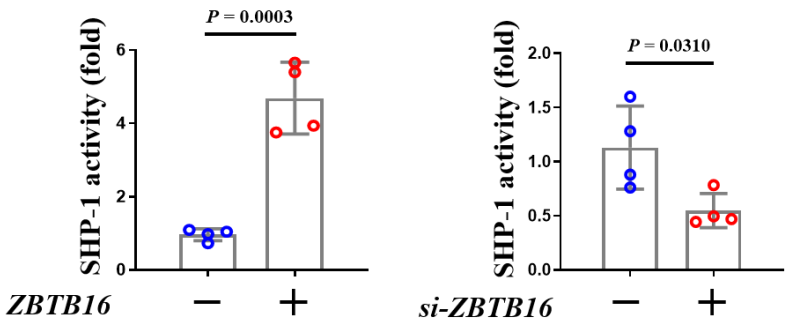


Figure 16. PLZF increases the transcriptional activity of SHP-1.

For the SHP-1 reporter assay, DU145 and LNCaP cells were transiently co-transfected with 1 $\mu$g of the *pGL3-PTPN6* promoter-luciferase reporter construct, *pcDNA3.1-ZBTB16* or *si-ZBTB16*, and *pCMV-$\beta$*-galactosidase. After 48 h, cells were lysed and luciferase activity was determined using luciferase reporter assay. All measurement values are normalized to that of $\beta$-galactosidase. Data represented as the means ± S.D. from 4 independent experiments [67].

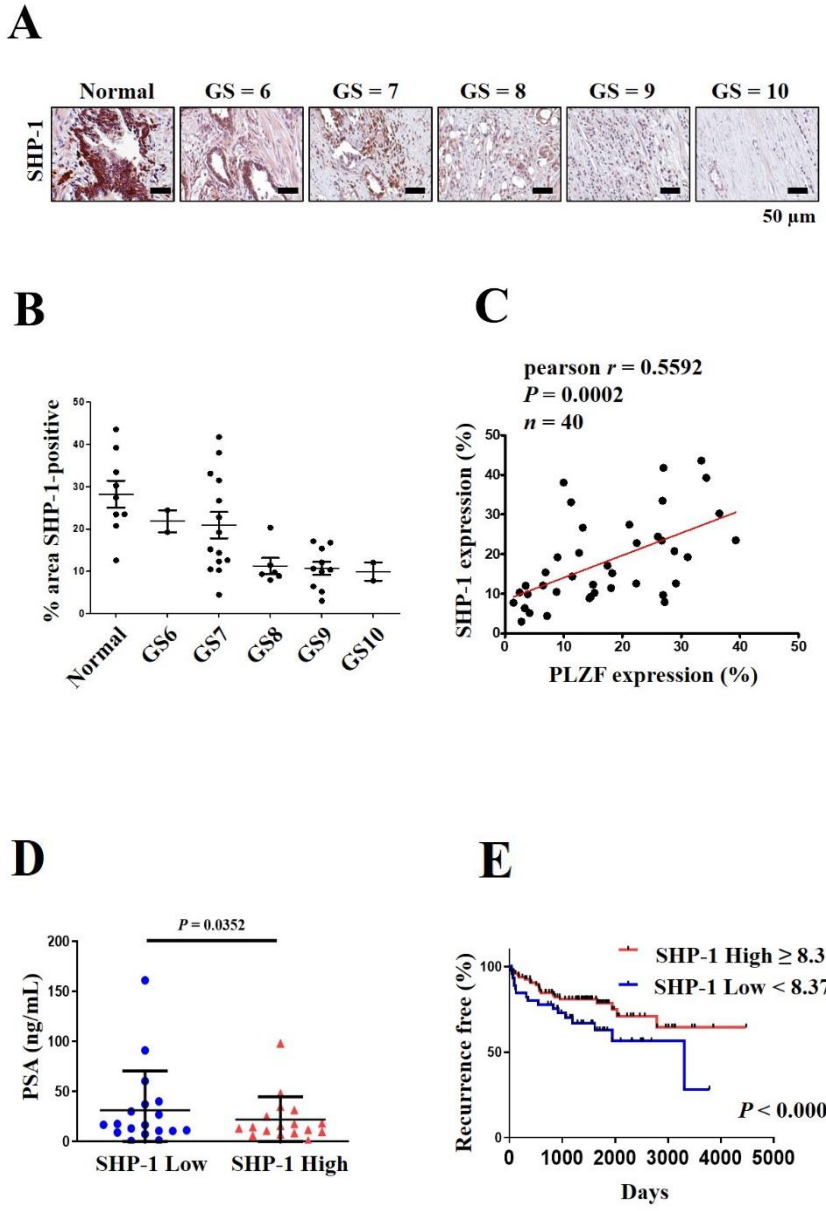
A
Normal
GS = 6
GS = 7
GS = 8
GS = 9
GS = 10
SHP-1
50 μm
B
% area SHP-1-positive
Normal
GS6
GS7
GS8
GS9
GS10
C
pearson r = 0.5592
P = 0.0002
n = 40
SHP-1 expression (%)
PLZF expression (%)
D
P = 0.0352
PSA (ng/mL)
SHP-1 Low
SHP-1 High
E
SHP-1 High ≥ 8.378 (n = 71)
SHP-1 Low < 8.378 (n = 70)
Recurrence free (%)
P < 0.0001
Days

**Figure 17. SHP-1 expression positively correlates with PLZF expression, and negatively correlates with high-grade GS and PSA pattern in prostate cancer patient tissues.**

(A) IHC staining in tissue arrays of surrounding normal prostate tissues and human prostate cancer specimens correlates with GS using anti-SHP-1 Abs. The images were visualized by Leica Aperio AT Turbo digital pathology scanner (magnification = 400×). (B) Quantification of SHP-1-positive expression according to the GS scores in benign ($n$ = 9) and malignant tumors ($n$ = 40). (C) Associations between SHP-1 and PLZF. Scatter plots showing the linear correlation determined by Pearson correlation coefficient calculation of those genes that were statistically significant. Pearson correlation coefficient $r$ and $P$-values are given in each scatter plot. (D) PSA levels were measured according to the SHP-1 ($P$ = 0.0352) protein levels, $n$ = 40. (E) SHP-1 expression inversely correlates with survival in prostate cancer patients. Recurrence free survival curves using Kaplan-Meier analysis when prostate cancer patients are divided into two groups based on median (high ≥ 8.378, low < 8.378) of the SHP-1 expression scores ($P$ < 0.0001). Data from the TCGA database [67].

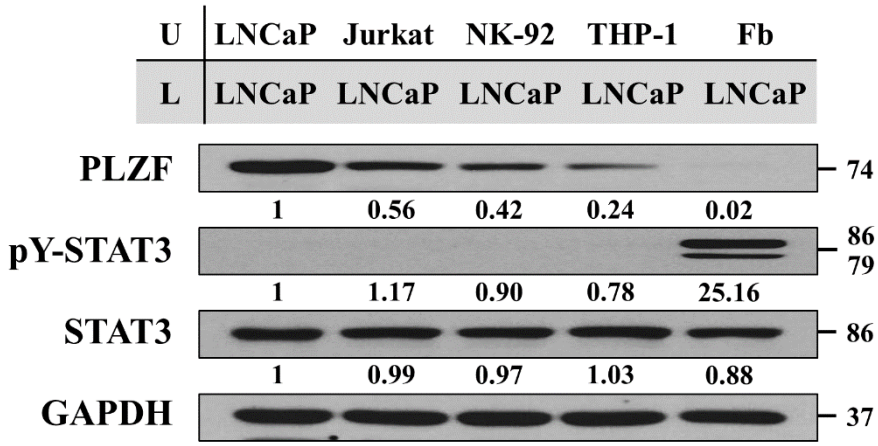


Figure 18. LNCaP cells co-cultured with fibroblasts inhibited PLZF most clearly among various stromal cells in the tumor microenvironment.

LNCaP cells co-cultured with Jurkat-T, NK-92, THP-1 and HDF(Fb, Fibroblast) for 24 h. LNCaP cells at low chamber were lysed for Western blotting. U: upper chamber, L: lower chamber. The band intensity of indicated proteins is expressed as a numerical value, relative to GAPDH [67].

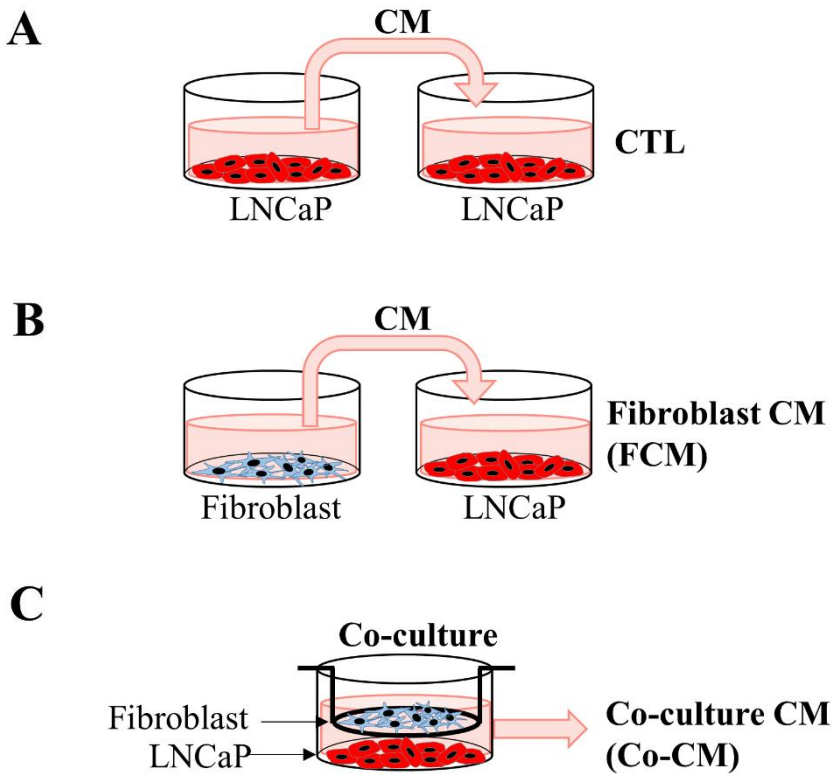


Figure 19. Schematic of the experimental set-up for conditioned media (CMs) treatment and the transwell co-culture system.

Conditioned media (CM) was prepared by incubating LNCaP (A, left, = CTL) and fibroblast (B, left, = FCM) cells in 10 mL per 100 mm dish for 48 h with serum free media. LNCaP cells were co-cultured with fibroblast using a cell culture chamber for 48 h (C, = Co-CM). Supernatant was collected and centrifuged at 13000 rpm for 3 min to remove the cell debris. LNCaP cells seeded in 6-well plate were converted into fresh media and then CTL or FCM was added. After 24 h of incubation or co-culture, cells at the 6-well plate bottom were harvested and used in the experiments [67].

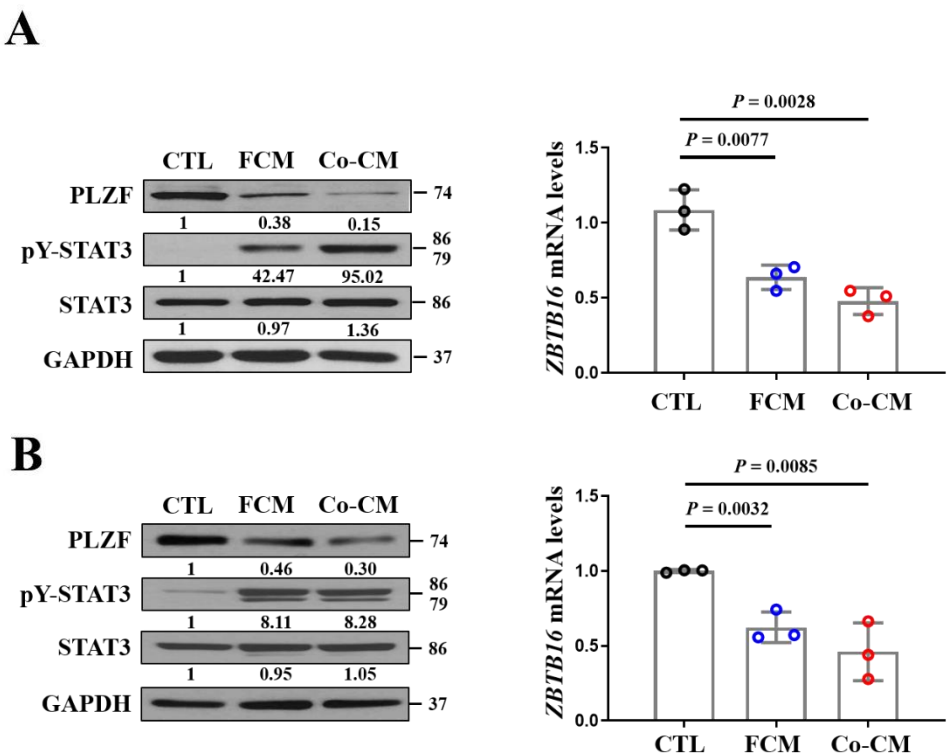


Figure 20. Protein and RNA expression of PLZF more reduce by direct co-culturing of fibroblast.

(A) LNCaP cells with FCM or Co-CM for 24 h. LNCaP cells were lysed for Western blotting (left). mRNA expression levels of *ZBTB16* were examined by qRT-PCR in LNCaP cells with FCM or Co-CM (right). (B) PLZF-transiently overexpressed DU145 cells with FCM or Co-CM for 24 h. DU145 cells were lysed for western blotting (left). mRNA expression levels of *ZBTB16* were examined by qRT-PCR in PLZF- transiently overexpressed DU145 cells with FCM or Co-CM (right). The band intensity of indicated proteins is expressed as a numerical value, relative to GAPDH. Data represented as the means ± S.D. from 3 independent experiments [67].

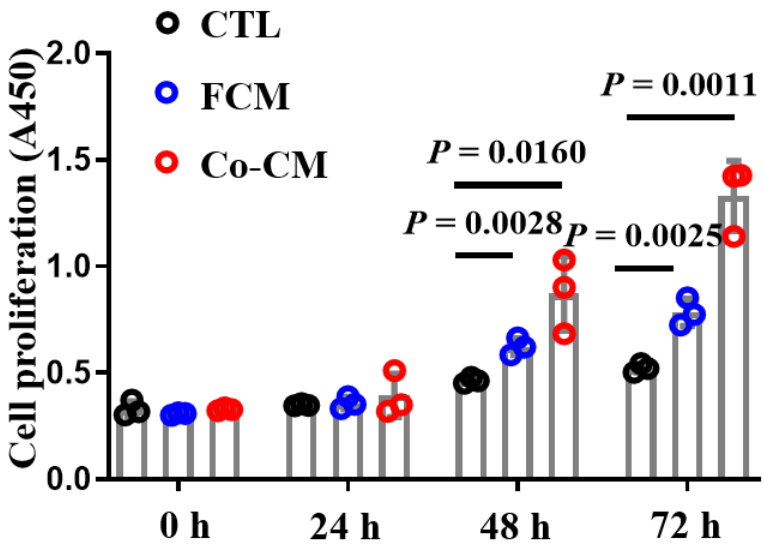


Figure 21. Conditioned media associated with fibroblast promotes prostate cancer cell proliferation.

Cell proliferation assay between FCM- and Co-CM- treated LNCaP cells were compared using a CCK assay. Cells were incubated for 24, 48, 72 h with CMs. Data represented as the means ± S.D. from 3 independent experiments [67].

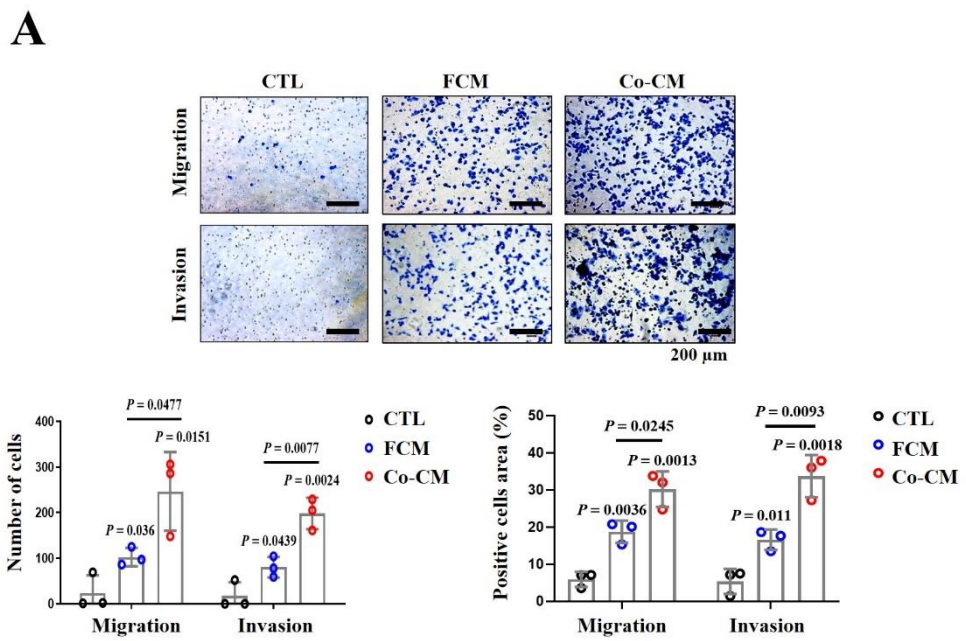
A
CTL
FCM
Co-CM
Migration
Invasion
200 μm
Number of cells
P = 0.0477
P = 0.0151
P = 0.036
P = 0.0077
P = 0.0024
P = 0.0439
CTL
FCM
Co-CM
Migration
Invasion
Positive cells area (%)
P = 0.0245
P = 0.0013
P = 0.0036
P = 0.0093
P = 0.0018
P = 0.011
CTL
FCM
Co-CM
Migration
Invasion

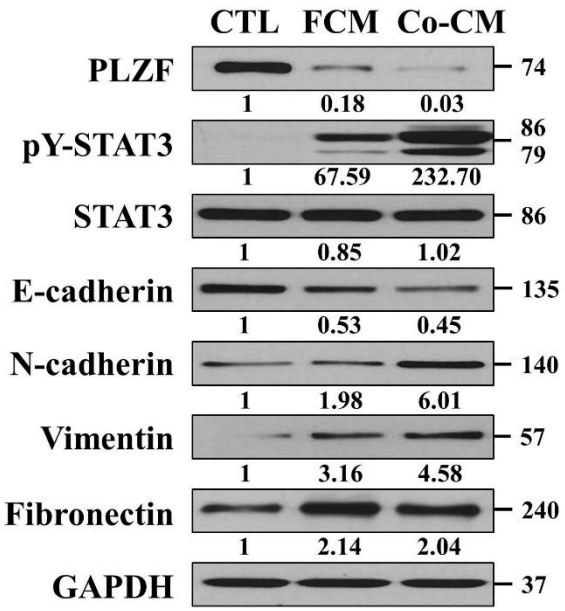
B
CTL FCM Co-CM
PLZF
74
1 0.18 0.03
pY-STAT3
86
79
1 67.59 232.70
STAT3
86
1 0.85 1.02
E-cadherin
135
1 0.53 0.45
N-cadherin
140
1 1.98 6.01
Vimentin
57
1 3.16 4.58
Fibronectin
240
1 2.14 2.04
GAPDH
37

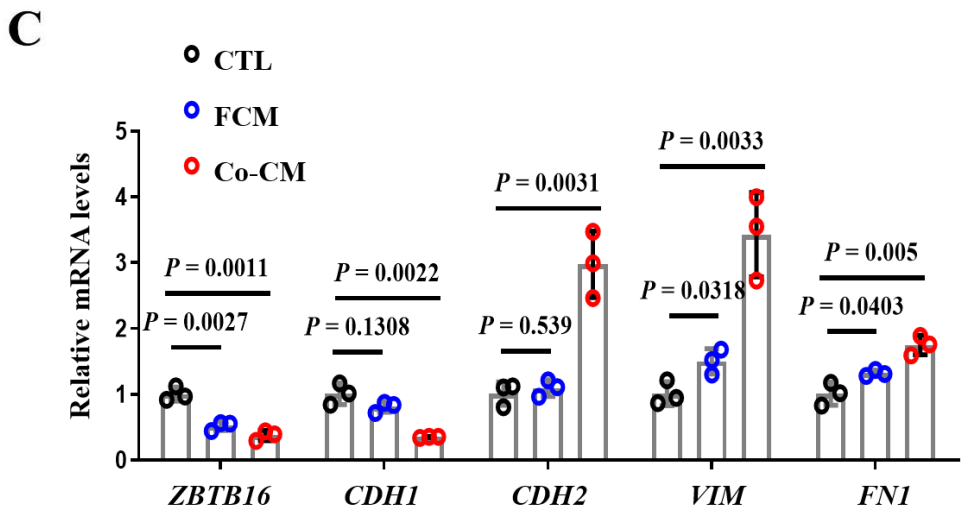


Figure 22. Conditioned media associated with fibroblast promotes the migration and invasion ability in prostate cancer cell lines by inhibiting PLZF.

(A) Transwell migration and matrigel invasion assays were conducted in LNCaP cells with FCM or Co-CM. The relative cell numbers are shown (bottom). The images (upper) were visualized by phase-contrast microscopy (magnification = 100×). The numbers (bottom, left) or the stained areas (bottom, right) of migrated and invaded cells are presented as bar graphs. (B) Protein expression levels of EMT markers in LNCaP cells with FCM or Co-CM. The band intensity of indicated proteins is expressed as a numerical value, relative to GAPDH. (C) mRNA expression levels of EMT markers were examined by qRT-PCR in LNCaP cells with FCM or Co-CM. Data represented as the means ± S.D. from 3 independent experiments [67].

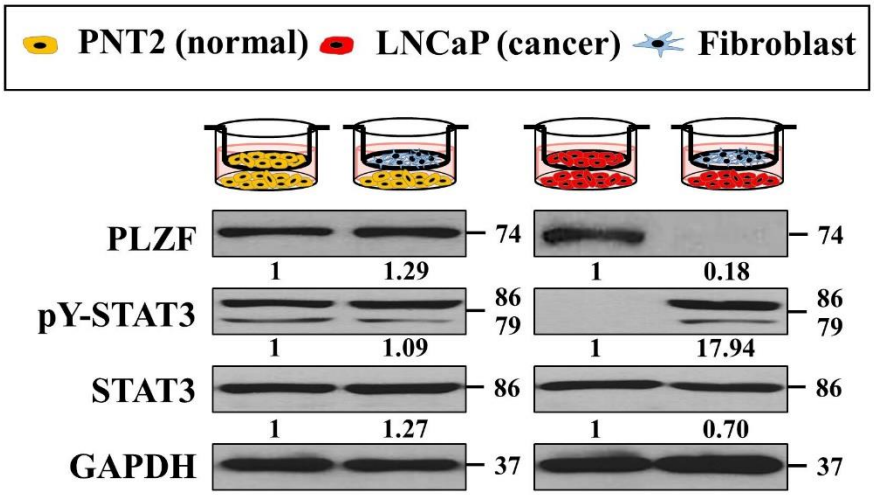


Figure 23. Fibroblasts affect PLZF and pY-STAT3 expressions of prostate cancer cells and non-prostate normal cells.

Prostate normal cells (PNT2) and prostate cancer cells (LNCaP) were co-cultured with fibroblast for 24 h. PLZF, pY-STAT3, STAT3, and GAPDH protein expression by Western blotting in LNCaP cells. The band intensity of indicated proteins is expressed as a numerical value, relative to GAPDH [67].

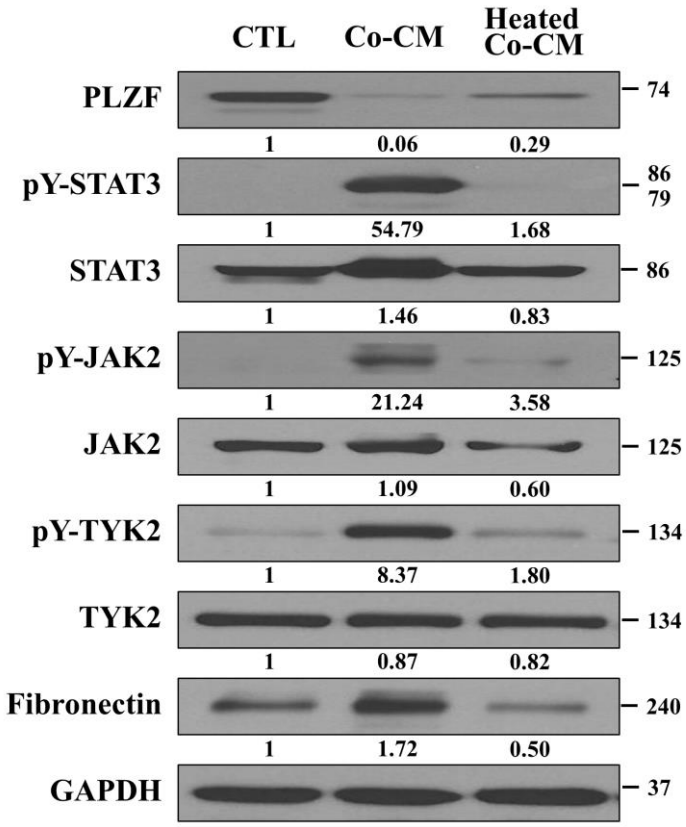


Figure 24. Fibroblast-induced effect was practically abolished by heated inactivation.

LNCaP cells were incubated with CTL, Co-CM, heated Co-CM for 24 h, and then cells were lysed for western blotting. Heated Co-CM was heated at 100℃ for 10 min. The band intensity of indicated proteins is expressed as a numerical value, relative to GAPDH [67].

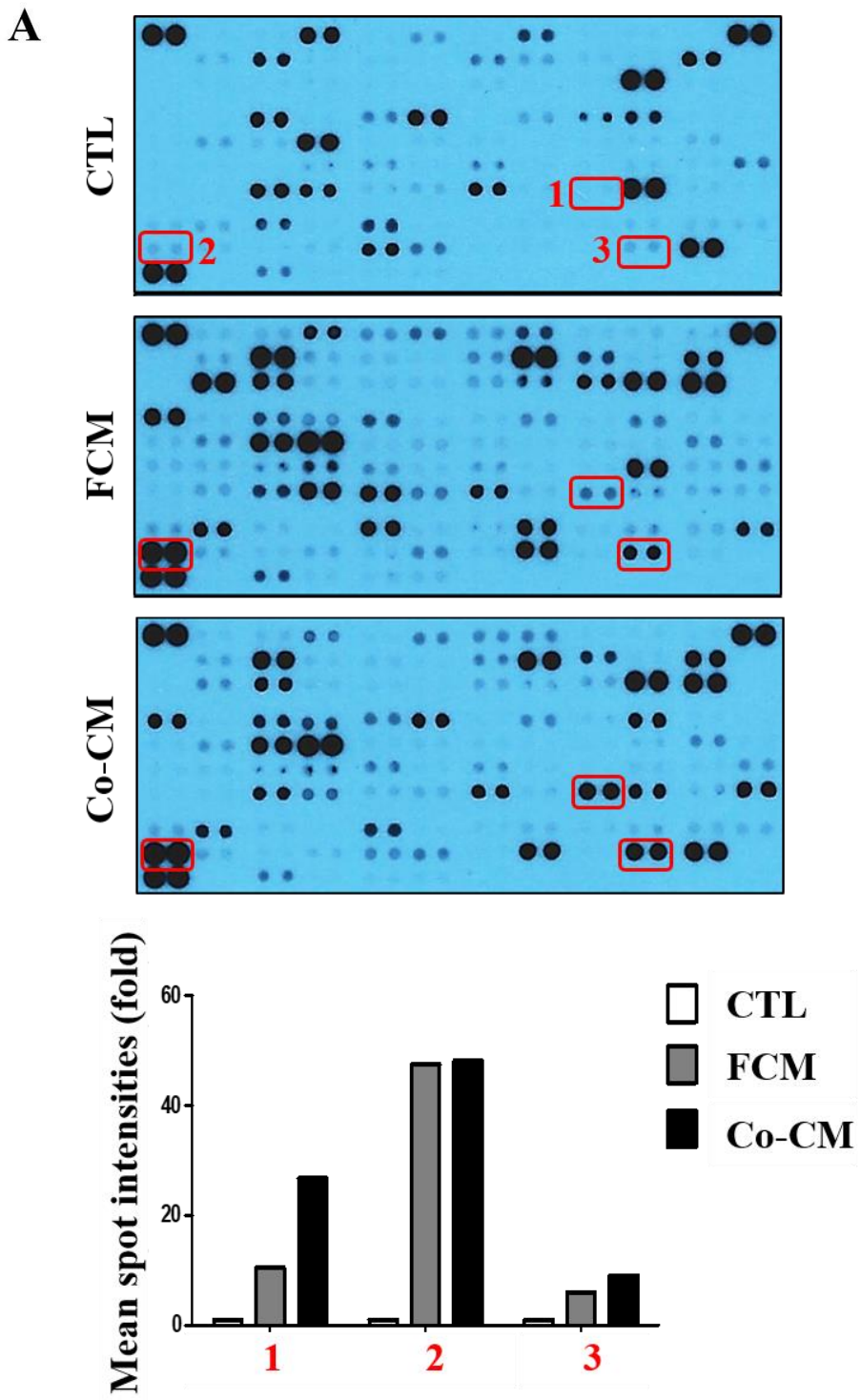


1: CCL3/4 2: SERPINE1 3: uPAR

**B**

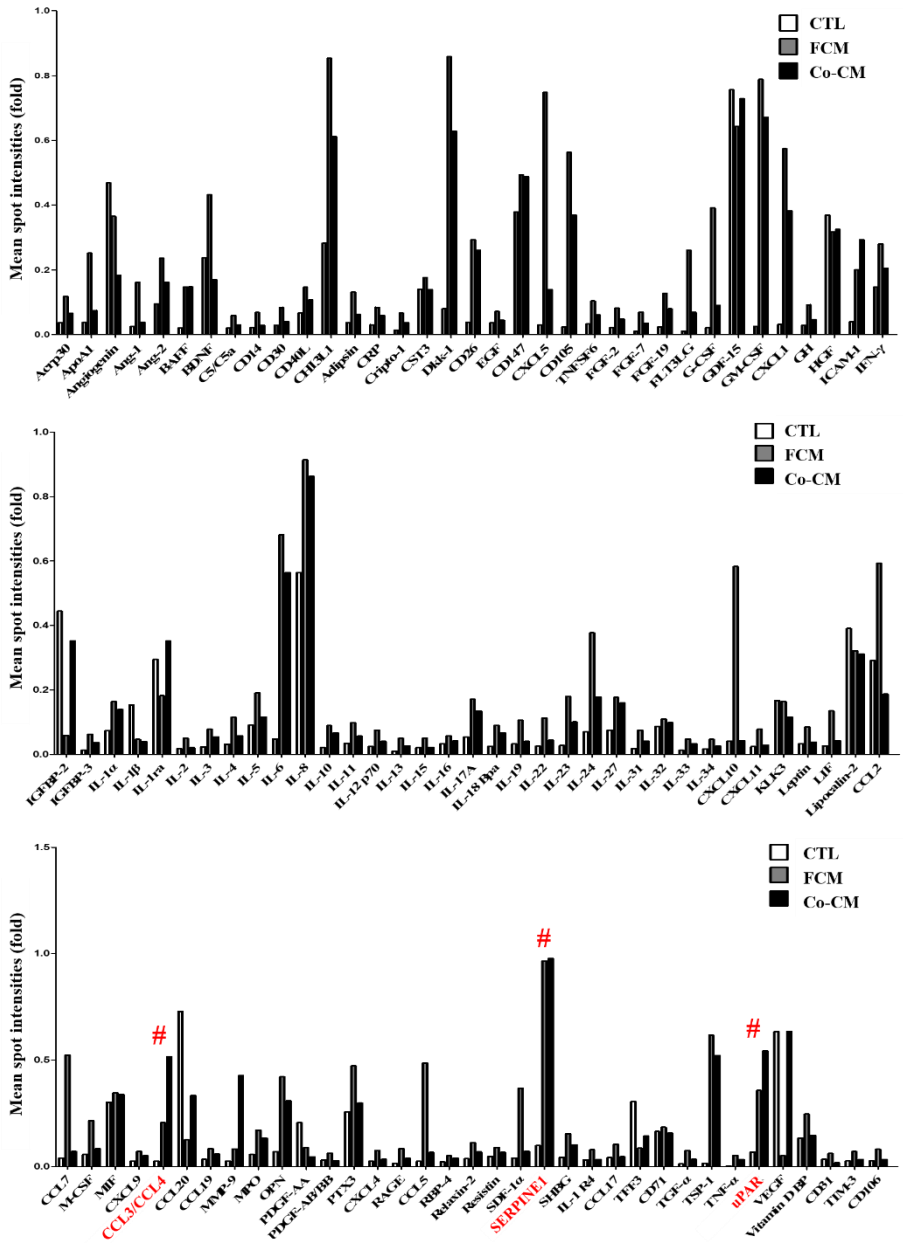
CTL
FCM
Co-CM
Mean spot intensities (fold)
Acrp30
ApoA1
Angiogenin
Ang-1
Ang-2
RAGE
BDNF
CSF/C5a
CD14
CD30
CD40L
CHI3L1
Adipsin
CRP
Cripto-1
CST3
Dkk-1
CD26
EGF
CD147
CXCL5
CD105
TNFSF6
FGF-2
FGF-7
FGF-19
FLT3LG
G-CSF
GDF-15
GM-CSF
CXCL1
GH
HGF
ICAM-1
IFN-γ
IGFBP-2
IGFBP-3
IL-1α
IL-1β
IL-1ra
IL-2
IL-3
IL-4
IL-5
IL-6
IL-8
IL-10
IL-11
IL-12 p70
IL-13
IL-15
IL-16
IL-17A
IL-18 Bpa
IL-19
IL-22
IL-23
IL-24
IL-27
IL-31
IL-32
IL-33
IL-34
CXCL10
CXCL11
KLK3
Leptin
LIF
Lipocalin-2
CCL2
CCL7
M-CSF
MIF
CXCL9
CCL3/CCL4
CCL20
CCL19
MMP-9
MPO
OPN
PDGF-AA
PDGF-ABBB
PTX3
CXCL4
RAGE
CCL5
RBP-4
Resistin-3
Resistin
SDF-1α
SERPINE1
SHBG
IL-1 R4
CCL17
TFF3
CD71
TGF-α
TSP-1
TNF-α
uPAR
VEGF
Vitamin D BP
CD31
TIM-3
CD106
#

Figure 25. Identification of tumor associated fibroblast-derived cytokines.

(A) Each CMs were applied to the cytokine arrays (top). CMs were collected for 48 h, and then cell debris was removed using the centrifuge. Membranes were developed using chemi-luminescence-type solution, and exposed to x-ray film. The positive signals seen on developed film can be identified by pairs of reference spots at three corners of each array. Also, expression level was normalized to positive biotinylated antibody signal spots and then to the CTL (A, upper) for each cytokine. The cytokines in red boxes are more enriched in Co-CM than in fibroblast CM. Fold change in mean spot intensity of cytokines are plotted (bottom). (B) The cytokine array contained 105 different capture antibodies. The mean pixel density of each dot on ARY022B antibody array was quantified using the Adobe Photoshop. Mean intensities of cytokines are plotted [67].

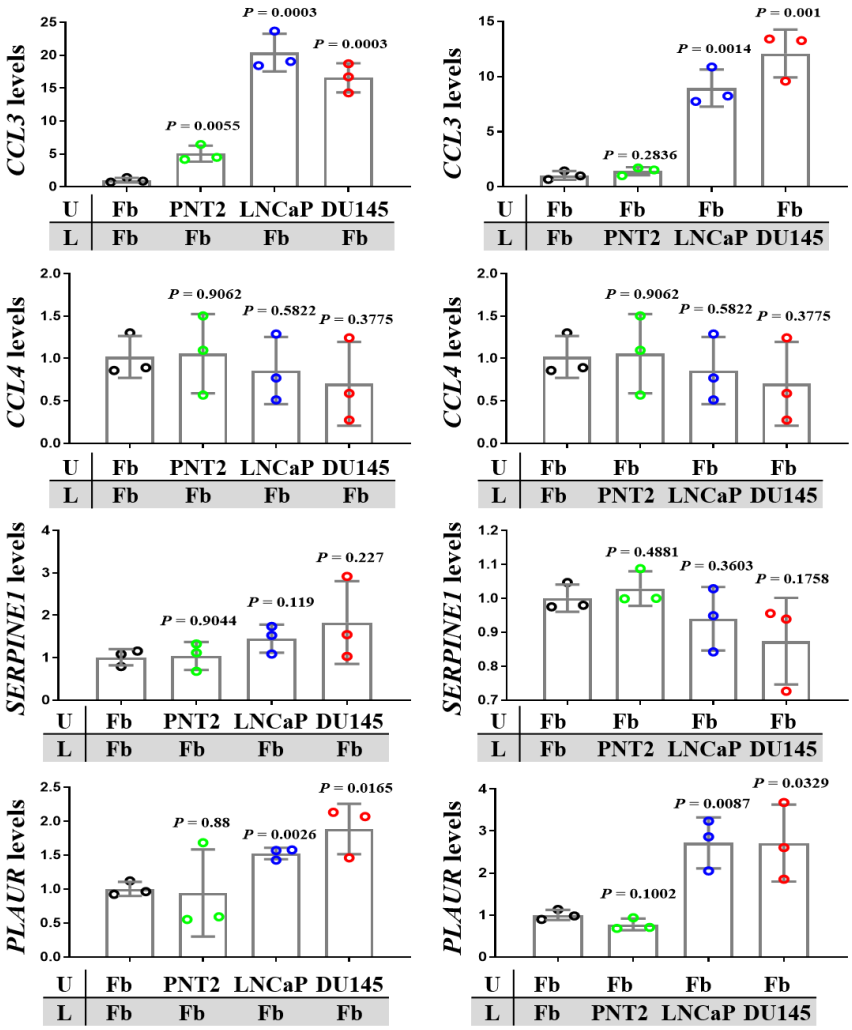


Figure 26. Fibroblasts visibly induced *CCL3* and *PLAUR* mRNA production by co-culturing with prostate cancer cells.

PNT2, LNCaP, and DU145 cells were co-cultured with fibroblast (Fb) in a cell culture chamber for 24 h. Cells in a lower chamber were lysed for qRT-PCR using the *CCL3*, *CCL4*, *SERPINE1* and *PLAUR* primers. U: upper chamber, L: lower chamber. Data represented as the means ± S.D. from 3 independent experiments [67].

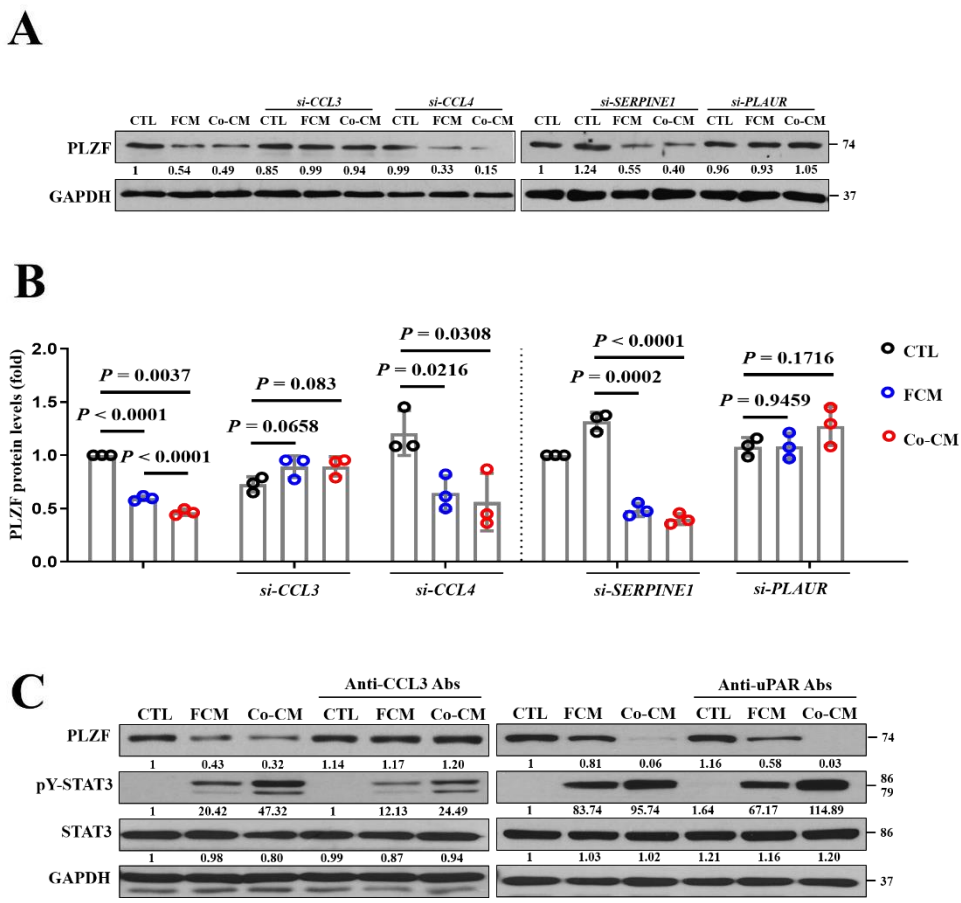
A
si-CCL3
si-CCL4
si-SERPINE1
si-PLAUR
CTL FCM Co-CM CTL FCM Co-CM CTL FCM Co-CM CTL CTL FCM Co-CM CTL FCM Co-CM
PLZF
74
1 0.54 0.49 0.85 0.99 0.94 0.99 0.33 0.15 1 1.24 0.55 0.40 0.96 0.93 1.05
GAPDH
37
B
PLZF protein levels (fold)
2.0
1.5
1.0
0.5
0.0
P = 0.0037
P < 0.0001
P < 0.0001
P = 0.083
P = 0.0658
P = 0.0308
P = 0.0216
P < 0.0001
P = 0.0002
P = 0.1716
P = 0.9459
si-CCL3
si-CCL4
si-SERPINE1
si-PLAUR
CTL
FCM
Co-CM
C
Anti-CCL3 Abs
Anti-uPAR Abs
CTL FCM Co-CM CTL FCM Co-CM CTL FCM Co-CM CTL FCM Co-CM
PLZF
74
1 0.43 0.32 1.14 1.17 1.20 1 0.81 0.06 1.16 0.58 0.03
pY-STAT3
86
79
1 20.42 47.32 1 12.13 24.49 1 83.74 95.74 1.64 67.17 114.89
STAT3
86
1 0.98 0.80 0.99 0.87 0.94 1 1.03 1.02 1.21 1.16 1.20
GAPDH
37

**Figure 27. Blocked CCL3 abolished the effect of PLZF caused by fibroblast.**

(A) LNCaP cells and fibroblast were transfected with 50nM of *si-CCL3, si-CCL4, si-SERPINE1, si-PLAUR*, respectively. After 48 h of transfection, a cultured media containing *si-RNA* was replaced with fresh media. Cells were incubated for 48 h, 10 mL per 100 mm dish with serum free media. Supernatant was collected and treated in LNCaP cells. The LNCaP cell lysates were subjected to western blotting for PLZF. The band intensity of indicated proteins is expressed as a numerical value, relative to GAPDH. (B) The levels of PLZF protein are presented as bar graphs. (C) CMs incubated with anti-CCL3 Abs or anti-uPAR Abs for 4 h were treated to LNCaP cells for 24 h. The LNCaP cell lysates were subjected to western blotting. The band intensity of indicated proteins is expressed as a numerical value, relative to GAPDH. Data represented as the means ± S.D. from 3 independent experiments [67].

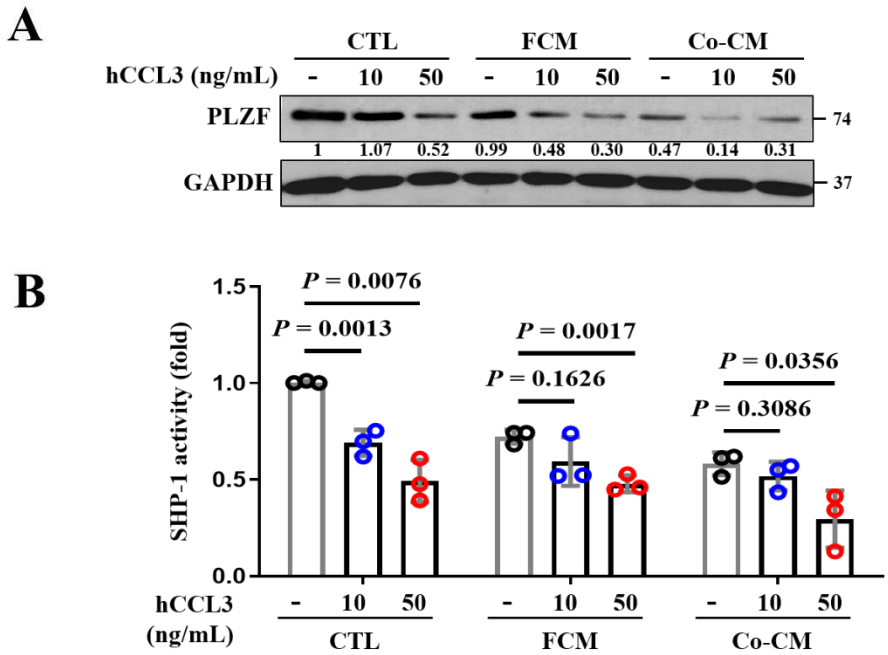


Figure 28. SHP-1-driven transcription is more inhibited with Co-CM than FCM by CCL3.

(A) Cells were treated with recombinant protein of CCL3 for 4 h and then treated with CMs for 24 h. PLZF protein expressions were subjected to western blotting. The band intensity of indicated proteins is expressed as a numerical value, relative to GAPDH. (B) LNCaP cells, which had been transfected with 1 $\mu$g of the *pGL3-PTPN6* promoter-luciferase reporter construct, were treated with CMs containing recombinant protein of CCL3. After 24 h, cells were lysed and luciferase activity was determined using luciferase reporter assay. All measurement values are normalized to that of $\beta$-galactosidase. Data represented as the means ± S.D. from 3 independent experiments [67].

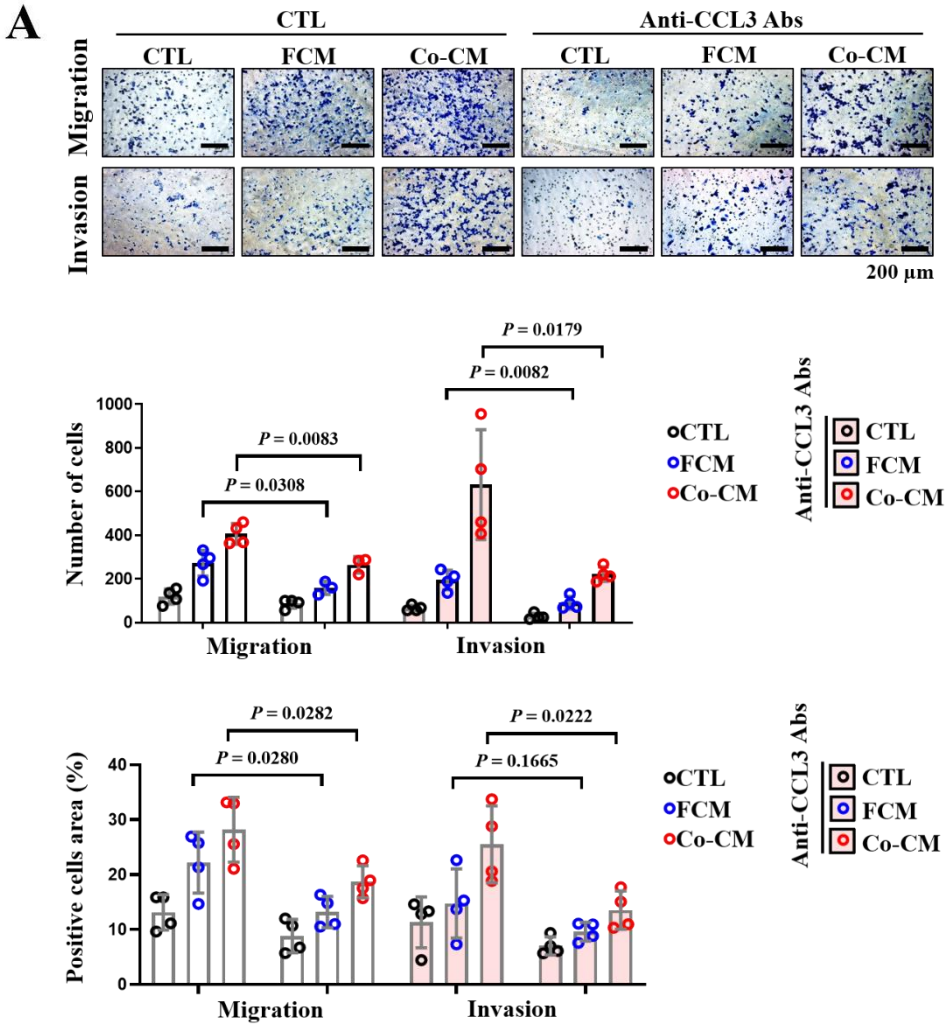
A
CTL
Anti-CCL3 Abs
CTL
FCM
Co-CM
CTL
FCM
Co-CM
Migration
Invasion
200 μm
P = 0.0179
P = 0.0082
P = 0.0083
P = 0.0308
Number of cells
1000
800
600
400
200
0
Migration
Invasion
CTL
FCM
Co-CM
Anti-CCL3 Abs
CTL
FCM
Co-CM
P = 0.0282
P = 0.0280
P = 0.0222
P = 0.1665
Positive cells area (%)
40
30
20
10
0
Migration
Invasion
CTL
FCM
Co-CM
Anti-CCL3 Abs
CTL
FCM
Co-CM

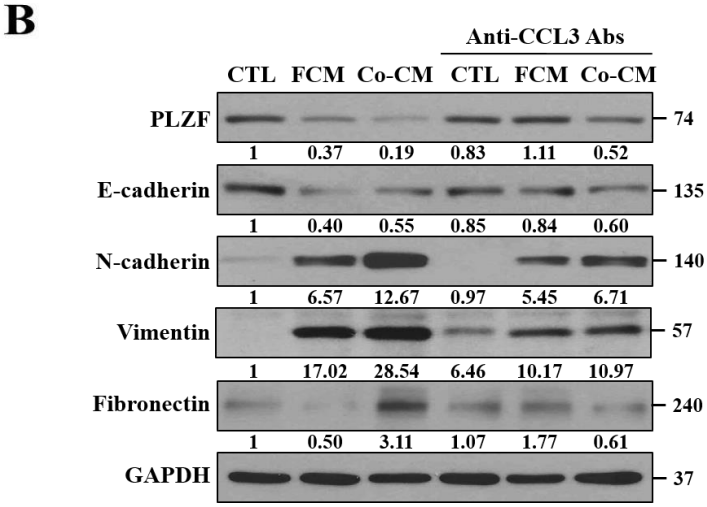
B
Anti-CCL3 Abs
CTL FCM Co-CM CTL FCM Co-CM
PLZF
74
1 0.37 0.19 0.83 1.11 0.52
E-cadherin
135
1 0.40 0.55 0.85 0.84 0.60
N-cadherin
140
1 6.57 12.67 0.97 5.45 6.71
Vimentin
57
1 17.02 28.54 6.46 10.17 10.97
Fibronectin
240
1 0.50 3.11 1.07 1.77 0.61
GAPDH
37

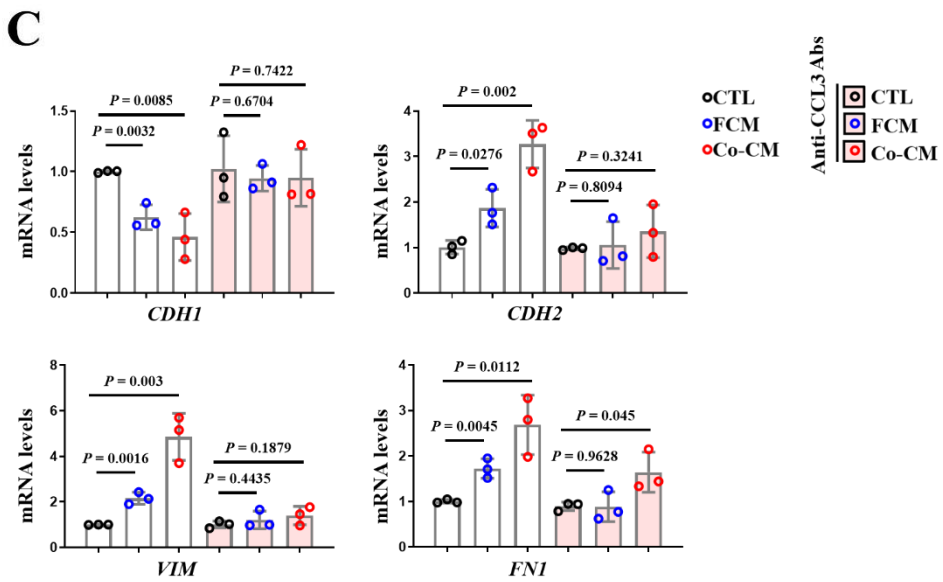


Figure 29. Blockade of CCL3 inhibited the fibroblast-induced migration and invasion of cancer cells.

(A) LNCaP cells were treated with recombinant protein of CCL3 for 4 h and then treated with CMs for 24 h. The images (upper) were visualized by phase-contrast microscopy (magnification = 100×). The numbers (middle) or the stained areas (bottom) of migrated and invaded cells are presented as bar graphs. Data represented as the means ± S.D. from 4 independent experiments. Levels of (B) protein and (C) mRNA in EMT markers (*CDH1, CDH2, VIM, FN1*) in LNCaP cells with CMs containing anti-CCL3 Abs. The LNCaP cell lysates were examined by (B) western blotting and (C) qRT-PCR. The band intensity of indicated proteins is expressed as a numerical value, relative to GAPDH. Data represented as the means ± S.D. from 3 independent experiments [67].

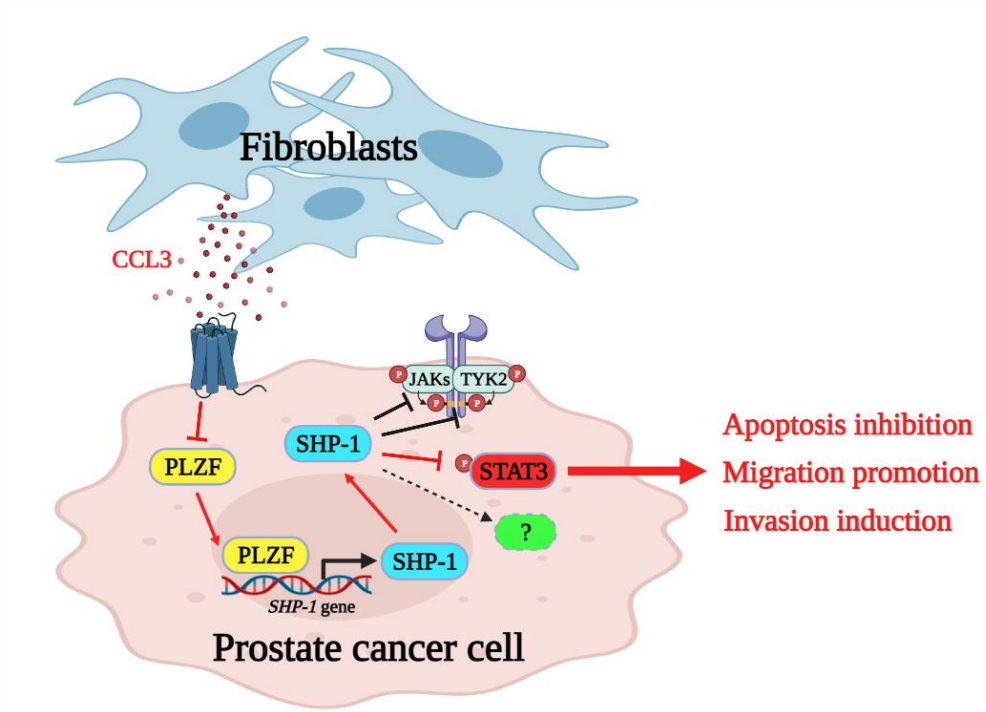


Figure 30. The mechanism of PLZF as a tumor suppressor in prostate cancer progression.

PLZF acts as a tumor suppressor to block cell viability, migration, and invasion in prostate cancer cells. Furthermore, prostate cancer cooperates with fibroblasts to collapse PLZF caused by CCL3 derived from fibroblasts. Mechanistic studies revealed that PLZF suppressed the JAKs-STAT3 pathway through reduction of SHP-1 [67].

# DISCUSSION

In this study, I discovered a new role for fibroblast in the prostate-tumor microenvironment to inhibit the tumor suppressor PLZF. While numerous reports have described the coevolution of stroma and prostate cancer cells in genotypic and phenotypic characters, some studies have elaborated on the contribution of fibroblasts that interacted with cancer to overall changes in gene and protein expression in prostate cancer microenvironments [40,41]. I identified for the first time a mechanism by which fibroblast-derived CCL3 suppresses PLZF expression, which promotes the synthesis of SHP-1 at the transcriptional levels, and then activates the JAKs-STAT3 pathway. PLZF was also significantly reduced in prostate cancer patient tissues, and low PLZF expression was found to correlate with GS and recurrence-free survival. Accordingly, down-regulation of PLZF activities can promote metastasis progression through improved growth and invasion of prostate cancer.

PLZF is a standard androgen-regulated putative tumor suppressor gene whose expression is suppressed by ADT. The reintroduction of PLZF expression is sufficient to restore androgen-independent growth mediated by PLZF depletion. Blocking androgen suppresses PLZF, a tumor suppressor gene, so cancer is progression [27,38]. Eventually, it can be expected that the mechanism of CRPC,

a cancer recurrence caused by resistance to ADT, which is an initial treatment method for prostate cancer, is due to inhibition of PLZF. Additionally, if CCL3 can be blocked to increase PLZF, there is a possibility of inhibiting CRPC, which is difficult to treat due to limited treatment methods.

I have identified how various oncogenes related to prostate tumor survival are altered by PLZF. It was surprisingly found that only tyrosine phosphorylation of JAKs-STAT3 was reduced, so I focused on tyrosine phosphatase SHP-1 related to STAT3. The cytoplasmic protein tyrosine phosphatase (PTP), characterized by containing two Src homology 2 (SH2) N-terminus, a single catalytic domain, and a C-terminal PTP domain, is referred to as SHP-1. The expression of SHP-1 in prostate cancer is inversely correlated with tumor stage and malignancy, as well as with biochemical recurrence after prostatectomy [35,42-44]. SHP-1 is known to have a tumor-suppressor role in various cancers due to the SHP-1-negative regulation of JAKs-STAT activation via growth factors and cytokines [44-47]. In addition, SHP-1 is associated with dephosphorylation of p27, PI3K/AKT, Cyclin E, and MAPKs as well as JAKs-STAT3 [48]. I found that SHP-1 transcription was promoted by PLZF, which reduced tyrosine phosphorylation of JAK2, TYK2 and STAT3. Collectively, these results suggest that PLZF can function with SHP-1 to reduce prostate cancer progression.

Cancer cells make use of the tremendous plastic nature of stromal cells, such as fibroblasts and macrophages, and produce

multiple signals that generate a tumor-promoting microenvironment [49-51]. Previous studies have indicated that co-culture or tumor cell CM could activate stromal fibroblasts, and tissue around fibroblasts were suggested as precursors for CAFs, activated by tumor cells [50-52]. In addition, fibroblasts are constantly exposed to different stimuli in the tumor microenvironment, facilitating unique features, such as excessive and specific secretion and the ECM remodeling phenotype [53,54]. Activated fibroblasts, i.e., CAFs, are involved in tumor invasiveness and metastasis by expressing a series of proteins that are not expressed by normal fibroblasts, such as α-smooth muscle actin (α-SMA) [55,56]. Moreover, contact between cancer cells and normal fibroblasts can facilitate the CAF phenotype in breast cancer through Notch signaling [57]. Various inflammatory modulators can promote CAF activation by interleukin-1 (IL-1), which acts through NF-κB and IL-6, which mainly acts on STATs [15]. Crosstalk and positive feedback involved in JAK-STAT signaling transduction, the contractile cytoskeleton, and alterations in histone acetylation further promote CAF activation [58,59]. It has been reported that CAFs promote tumor growth by directly stimulating tumor cell proliferation, play an important role in wound healing, and mediate other aspects of complex processes such as ECM remodeling [10,15,60]. Moreover, CAFs contribute to tumor progression by providing cancer cells with growth factors and pro-inflammatory tumor-promoting microenvironments [15,33,61].

This study need to be understood in the context of the following

methodological limitations. HDFs were used as controls or "normally" stromal cells to determine interactions with cancer, but they are not complete normal cells because they are immortalized cell line. Therefore, as shown in figure 20-29, I think that there is a slight change in the prostate cancer cells even by FCM. Furthermore, there is a weakness in that the normal HDFs has not experimentally clearly demonstrated the transition to the CAFs. Nevertheless, there are several references [15,51,60-64] to support my experimental results. Although less than CAF, there is a report that normal fibroblasts also promote lung cancer more malignant by confirming that it also expresses FAP [62]. Normal fibroblasts can exert various of promoting functions against cancer initiating and metastatic cells by differentiating into CAF through co-culture, direct cell-cell contact, paracrine signaling by soluble factors, and ECM integrity [53,63,64]. In addition, FGF exposure of HDF, which is a normal fibroblast, is activated, and thus the proliferation and self-renewal effect of skin squamous cell carcinomas is increased [65]. Interestingly, mixing normal skin fibroblasts and carcinoma cells resulted in tumor growth that was slower than tumors mixed with CAF but significantly greater than tumor cells alone [15]. CAF can be derived from the activation of normal fibroblasts mediated by growth factors released from tumor cells. In addition, tumor cells can regulate fibroblast behavior through the release of EVs that induce phenotypic and functional changes in normal stromal fibroblasts and activate them in a CAF-like state. These CAF-like cells can in turn stimulate some abilities in surrounding normal and tumor cells [66].

Through this, the possibility of obtaining a CAF-like phenotype was confirmed by exposing HDF, normal fibroblast, to prostate cancer cells. Taken together, current findings suggest a crucial mechanism involving positive feedback between fibroblast and cancer cells, and this mechanism is essential for the progression and metastasis of prostate cancer (Figure 30).

In conclusion, PLZF is not only one of the most commonly under-expressed putative driver genes in prostate cancer, but its expression levels are closely linked with key mechanisms of prostate cancer progression. Also, this study provides a rational mechanism to support the clinical evidence for tumor microenvironment-induced malignancies. Results suggest that targeting PLZF may aid in predicting metastasis risk in cancer patients. That is, from a therapeutic point of view, the PLZF signaling pathway could be a potential target for preventing cancer metastasis.

# REFERENCE


1. Siegel, R.L.; Miller, K.D.; Jemal, A. Cancer statistics, 2020. *CA Cancer J Clin* 2020, *70*, 7–30, doi:10.3322/caac.21590.

2. Gundem, G.; Van Loo, P.; Kremeyer, B.; Alexandrov, L.B.; Tubio, J.M.C.; Papaemmanuil, E.; Brewer, D.S.; Kallio, H.M.L.; Högnäs, G.; Annala, M.; et al. The evolutionary history of lethal metastatic prostate cancer. *Nature* 2015, *520*, 353–357, doi:10.1038/nature14347.

3. Harryman, W.L.; Hinton, J.P.; Rubenstein, C.P.; Singh, P.; Nagle, R.B.; Parker, S.J.; Knudsen, B.S.; Cress, A.E. The Cohesive Metastasis Phenotype in Human Prostate Cancer. *Biochim Biophys Acta* 2016, *1866*, 221–231, doi:10.1016/j.bbcan.2016.09.005.

4. Cheng, Y.; Gao, X.H.; Li, X.J.; Cao, Q.H.; Zhao, D.D.; Zhou, J.R.; Wu, H.X.; Wang, Y.; You, L.J.; Yang, H.B.; et al. Depression promotes prostate cancer invasion and metastasis via a sympathetic–cAMP–FAK signaling pathway. *Oncogene* 2018, *37*, 2953–2966, doi:10.1038/s41388–018–0177–4.

5. Birnbaum, M.D.; Zhao, N.; Moorthy, B.T.; Patel, D.M.; Kryvenko, O.N.; Heidman, L.; Kumar, A.; Morgan, W.M.; Ban,

Y.; Reis, I.M.; et al. Reduced Arginyltransferase 1 is a driver and a potential prognostic indicator of prostate cancer metastasis. *Oncogene* **2019**, *38*, 838-851, doi:10.1038/s41388-018-0462-2.

6. Hanahan, D.; Weinberg, R.A. Hallmarks of cancer: the next generation. *Cell* **2011**, *144*, 646-674, doi:10.1016/j.cell.2011.02.013.

7. Hanahan, D.; Coussens, L.M. Accessories to the crime: functions of cells recruited to the tumor microenvironment. *Cancer Cell* **2012**, *21*, 309-322, doi:10.1016/j.ccr.2012.02.022.

8. Cheteh, E.H.; Augsten, M.; Rundqvist, H.; Bianchi, J.; Sarne, V.; Egevad, L.; Bykov, V.J.; Östman, A.; Wiman, K.G. Human cancer-associated fibroblasts enhance glutathione levels and antagonize drug-induced prostate cancer cell death. *Cell Death Dis* **2017**, *8*, e2848, doi:10.1038/cddis.2017.225.

9. Qiu, W.; Hu, M.; Sridhar, A.; Opeskin, K.; Fox, S.; Shipitsin, M.; Trivett, M.; Thompson, E.R.; Ramakrishna, M.; Gorringe, K.L.; et al. No evidence of clonal somatic genetic alterations in cancer-associated fibroblasts from human breast and ovarian carcinomas. *Nat Genet* **2008**, *40*, 650-655, doi:10.1038/ng.117.

10. Allinen, M.; Beroukhim, R.; Cai, L.; Brennan, C.; Lahti-

Domenici, J.; Huang, H.; Porter, D.; Hu, M.; Chin, L.; Richardson, A.; et al. Molecular characterization of the tumor microenvironment in breast cancer. *Cancer Cell* 2004, *6*, 17-32, doi:10.1016/j.ccr.2004.06.010.

11. Gascard, P.; Tlsty, T.D. Carcinoma-associated fibroblasts: orchestrating the composition of malignancy. *Genes Dev* 2016, *30*, 1002-1019, doi:10.1101/gad.279737.116.

12. Bu, L.; Baba, H.; Yoshida, N.; Miyake, K.; Yasuda, T.; Uchihara, T.; Tan, P.; Ishimoto, T. Biological heterogeneity and versatility of cancer-associated fibroblasts in the tumor microenvironment. *Oncogene* 2019, *38*, 4887-4901, doi:10.1038/s41388-019-0765-y.

13. Trimboli, A.J.; Cantemir-Stone, C.Z.; Li, F.; Wallace, J.A.; Merchant, A.; Creasap, N.; Thompson, J.C.; Caserta, E.; Wang, H.; Chong, J.L.; et al. Pten in stromal fibroblasts suppresses mammary epithelial tumours. *Nature* 2009, *461*, 1084-1091, doi:10.1038/nature08486.

14. Bhowmick, N.A.; Neilson, E.G.; Moses, H.L. Stromal fibroblasts in cancer initiation and progression. *Nature* 2004, *432*, 332-337, doi:10.1038/nature03096.

15. Erez, N.; Truitt, M.; Olson, P.; Arron, S.T.; Hanahan, D. Cancer-Associated Fibroblasts Are Activated in Incipient Neoplasia to Orchestrate Tumor-Promoting Inflammation in

an NF-kappaB-Dependent Manner. *Cancer Cell* 2010, *17*, 135-147, doi:10.1016/j.ccr.2009.12.041.

16. Suliman, B.A.; Xu, D.; Williams, B.R. The promyelocytic leukemia zinc finger protein: two decades of molecular oncology. *Front Oncol* 2012, *2*, 74, doi:10.3389/fonc.2012.00074.

17. Xiao, G.Q.; Unger, P.; Yang, Q.; Kinoshita, Y.; Singh, K.; McMahon, L.; Nastiuk, K.; Sha, K.; Krolewski, J.; Burstein, D. Loss of PLZF expression in prostate cancer by immunohistochemistry correlates with tumor aggressiveness and metastasis. *PLoS One* 2015, *10*, e0121318, doi:10.1371/journal.pone.0121318.

18. Liu, T.M.; Lee, E.H.; Lim, B.; Shyh-Chang, N. Concise Review: Balancing Stem Cell Self-Renewal and Differentiation with PLZF. *Stem Cells* 2016, *34*, 277-287, doi:10.1002/stem.2270.

19. Shen, H.; Zhan, M.; Zhang, Y.; Huang, S.; Xu, S.; Huang, X.; He, M.; Yao, Y.; Man, M.; Wang, J. PLZF inhibits proliferation and metastasis of gallbladder cancer by regulating IFIT2. *Cell Death Dis* 2018, *9*, 71, doi:10.1038/s41419-017-0107-3.

20. Kovalovsky, D.; Uche, O.U.; Eladad, S.; Hobbs, R.M.; Yi, W.; Alonzo, E.; Chua, K.; Eidson, M.; Kim, H.J.; Im, J.S.; et al. The BTB-zinc finger transcriptional regulator PLZF controls the

development of invariant natural killer T cell effector functions. *Nat Immunol* 2008, *9*, 1055-1064, doi:10.1038/ni.1641.

21. Savage, A.K.; Constantinides, M.G.; Han, J.; Picard, D.; Martin, E.; Li, B.; Lantz, O.; Bendelac, A. The transcription factor PLZF directs the effector program of the NKT cell lineage. *Immunity* 2008, *29*, 391-403, doi:10.1016/j.immuni.2008.07.011.

22. Eidson, M.; Wahlstrom, J.; Beaulieu, A.M.; Zaidi, B.; Carsons, S.E.; Crow, P.K.; Yuan, J.; Wolchok, J.D.; Horsthemke, B.; Wieczorek, D.; et al. Altered development of NKT cells, γδ T cells, CD8 T cells and NK cells in a PLZF deficient patient. *PLoS One* 2011, *6*, e24441, doi:10.1371/journal.pone.0024441.

23. McConnell, M.J.; Chevallier, N.; Berkofsky-Fessler, W.; Giltnane, J.M.; Malani, R.B.; Staudt, L.M.; Licht, J.D. Growth suppression by acute promyelocytic leukemia-associated protein PLZF is mediated by repression of c-myc expression. *Mol Cell Biol* 2003, *23*, 9375-9388, doi:10.1128/mcb.23.24.9375-9388.2003.

24. Felicetti, F.; Bottero, L.; Felli, N.; Mattia, G.; Labbaye, C.; Alvino, E.; Peschle, C.; Colombo, M.P.; Carè, A. Role of PLZF in melanoma progression. *Oncogene* 2004, *23*, 4567-4576,

doi:10.1038/sj.onc.1207597.

25. Cheung, M.; Pei, J.; Pei, Y.; Jhanwar, S.C.; Pass, H.I.; Testa, J.R. The promyelocytic leukemia zinc-finger gene, PLZF, is frequently downregulated in malignant mesothelioma cells and contributes to cell survival. *Oncogene* 2010, *29*, 1633-1640, doi:10.1038/onc.2009.455.

26. Wang, X.; Wang, L.; Guo, S.; Bao, Y.; Ma, Y.; Yan, F.; Xu, K.; Xu, Z.; Jin, L.; Lu, D.; et al. Hypermethylation reduces expression of tumor-suppressor PLZF and regulates proliferation and apoptosis in non-small-cell lung cancers. *Faseb j* 2013, *27*, 4194-4203, doi:10.1096/fj.13-229070.

27. Hsieh, C.L.; Botta, G.; Gao, S.; Li, T.; Van Allen, E.M.; Treacy, D.J.; Cai, C.; He, H.H.; Sweeney, C.J.; Brown, M.; et al. PLZF, a tumor suppressor genetically lost in metastatic castration-resistant prostate cancer, is a mediator of resistance to androgen deprivation therapy. *Cancer Res* 2015, *75*, 1944-1948, doi:10.1158/0008-5472.Can-14-3602.

28. Cao, J.; Zhu, S.; Zhou, W.; Li, J.; Liu, C.; Xuan, H.; Yan, J.; Zheng, L.; Zhou, L.; Yu, J.; et al. PLZF mediates the PTEN/AKT/FOXO3a signaling in suppression of prostate tumorigenesis. *PLoS One* 2013, *8*, e77922, doi:10.1371/journal.pone.0077922.

29. Stopsack, K.H.; Gerke, T.; Tyekucheva, S.; Mazzu, Y.Z.; Lee,

G.M.; Chakraborty, G.; Abida, W.; Mucci, L.A.; Kantoff, P.W. Low Expression of the Androgen-Induced Tumor Suppressor Gene PLZF and Lethal Prostate Cancer. *Cancer Epidemiol Biomarkers Prev* 2019, *28*, 707-714, doi:10.1158/1055-9965.Epi-18-1014.

30. Menten, P.; Wuyts, A.; Van Damme, J. Macrophage inflammatory protein-1. *Cytokine Growth Factor Rev* 2002, *13*, 455-481, doi:10.1016/s1359-6101(02)00045-x.

31. da Silva, J.M.; Moreira Dos Santos, T.P.; Sobral, L.M.; Queiroz-Junior, C.M.; Rachid, M.A.; Proudfoot, A.E.I.; Garlet, G.P.; Batista, A.C.; Teixeira, M.M.; Leopoldino, A.M.; et al. Relevance of CCL3/CCR5 axis in oral carcinogenesis. *Oncotarget* 2017, *8*, 51024-51036, doi:10.18632/oncotarget.16882.

32. Wu, Y.; Li, Y.Y.; Matsushima, K.; Baba, T.; Mukaida, N. CCL3-CCR5 axis regulates intratumoral accumulation of leukocytes and fibroblasts and promotes angiogenesis in murine lung metastasis process. *J Immunol* 2008, *181*, 6384-6393, doi:10.4049/jimmunol.181.9.6384.

33. Tanabe, Y.; Sasaki, S.; Mukaida, N.; Baba, T. Blockade of the chemokine receptor, CCR5, reduces the growth of orthotopically injected colon cancer cells via limiting cancer-associated fibroblast accumulation. *Oncotarget* 2016, *7*, 48335-48345, doi:10.18632/oncotarget.10227.

34. Sasaki, S.; Baba, T.; Shinagawa, K.; Matsushima, K.; Mukaida, N. Crucial involvement of the CCL3-CCR5 axis-mediated fibroblast accumulation in colitis-associated carcinogenesis in mice. *Int J Cancer* 2014, *135*, 1297-1306, doi:10.1002/ijc.28779.

35. Chong, Z.Z.; Maiese, K. The Src homology 2 domain tyrosine phosphatases SHP-1 and SHP-2: diversified control of cell growth, inflammation, and injury. *Histol Histopathol* 2007, *22*, 1251-1267, doi:10.14670/hh-22.1251.

36. Jiang, F.; Wang, Z. Identification and characterization of PLZF as a prostatic androgen-responsive gene. *Prostate* 2004, *59*, 426-435, doi:10.1002/pros.20000.

37. Kikugawa, T.; Kinugasa, Y.; Shiraishi, K.; Nanba, D.; Nakashiro, K.; Tanji, N.; Yokoyama, M.; Higashiyama, S. PLZF regulates Pbx1 transcription and Pbx1-HoxC8 complex leads to androgen-independent prostate cancer proliferation. *Prostate* 2006, *66*, 1092-1099, doi:10.1002/pros.20443.

38. Jin, Y.; Nenseth, H.Z.; Saatcioglu, F. Role of PLZF as a tumor suppressor in prostate cancer. *Oncotarget* 2017, *8*, 71317-71324, doi:10.18632/oncotarget.19813.

39. Kalluri, R.; Zeisberg, M. Fibroblasts in cancer. *Nat Rev Cancer* 2006, *6*, 392-401, doi:10.1038/nrc1877.

40. Kansy, B.A.; Dißmann, P.A.; Hemeda, H.; Bruderek, K.; Westerkamp, A.M.; Jagalski, V.; Schuler, P.; Kansy, K.; Lang, S.; Dumitru, C.A.; et al. The bidirectional tumor--mesenchymal stromal cell interaction promotes the progression of head and neck cancer. *Stem Cell Res Ther* 2014, *5*, 95, doi:10.1186/scrt484.

41. Hughes, R.M.; Simons, B.W.; Khan, H.; Miller, R.; Kugler, V.; Torquato, S.; Theodros, D.; Haffner, M.C.; Lotan, T.; Huang, J.; et al. Asporin Restricts Mesenchymal Stromal Cell Differentiation, Alters the Tumor Microenvironment, and Drives Metastatic Progression. *Cancer Res* 2019, *79*, 3636-3650, doi:10.1158/0008-5472.Can-18-2931.

42. Nunes-Xavier, C.E.; Mingo, J.; López, J.I.; Pulido, R. The role of protein tyrosine phosphatases in prostate cancer biology. *Biochim Biophys Acta Mol Cell Res* 2019, *1866*, 102-113, doi:10.1016/j.bbamcr.2018.06.016.

43. Cariaga-Martinez, A.E.; Lorenzati, M.A.; Riera, M.A.; Cubilla, M.A.; De La Rossa, A.; Giorgio, E.M.; Tiscornia, M.M.; Gimenez, E.M.; Rojas, M.E.; Chaneton, B.J.; et al. Tumoral prostate shows different expression pattern of somatostatin receptor 2 (SSTR2) and phosphotyrosine phosphatase SHP-1 (PTPN6) according to tumor progression. *Adv Urol* 2009, *2009*, 723831, doi:10.1155/2009/723831.

44. Zapata, P.D.; Ropero, R.M.; Valencia, A.M.; Buscail, L.; López, J.I.; Martín-Orozco, R.M.; Prieto, J.C.; Angulo, J.; Susini, C.; López-Ruiz, P.; et al. Autocrine regulation of human prostate carcinoma cell proliferation by somatostatin through the modulation of the SH2 domain containing protein tyrosine phosphatase (SHP)-1. *J Clin Endocrinol Metab* 2002, *87*, 915-926, doi:10.1210/jcem.87.2.8194.

45. Tassidis, H.; Culig, Z.; Wingren, A.G.; Härkönen, P. Role of the protein tyrosine phosphatase SHP-1 in Interleukin-6 regulation of prostate cancer cells. *Prostate* 2010, *70*, 1491-1500, doi:10.1002/pros.21184.

46. Tassidis, H.; Brokken, L.J.; Jirström, K.; Ehrnström, R.; Pontén, F.; Ulmert, D.; Bjartell, A.; Härkönen, P.; Wingren, A.G. Immunohistochemical detection of tyrosine phosphatase SHP-1 predicts outcome after radical prostatectomy for localized prostate cancer. *Int J Cancer* 2010, *126*, 2296-2307, doi:10.1002/ijc.24917.

47. Huang, T.T.; Su, J.C.; Liu, C.Y.; Shiau, C.W.; Chen, K.F. Alteration of SHP-1/p-STAT3 Signaling: A Potential Target for Anticancer Therapy. *Int J Mol Sci* 2017, *18*, doi:10.3390/ijms18061234.

48. Varone, A.; Spano, D.; Corda, D. Shp1 in Solid Cancers and Their Therapy. *Front Oncol* 2020, *10*, 935,

doi:10.3389/fonc.2020.00935.

49. Wang, W.; Yang, X.; Dai, J.; Lu, Y.; Zhang, J.; Keller, E.T. Prostate cancer promotes a vicious cycle of bone metastasis progression through inducing osteocytes to secrete GDF15 that stimulates prostate cancer growth and invasion. *Oncogene* 2019, *38*, 4540-4559, doi:10.1038/s41388-019-0736-3.

50. Sharon, Y.; Raz, Y.; Cohen, N.; Ben-Shmuel, A.; Schwartz, H.; Geiger, T.; Erez, N. Tumor-derived osteopontin reprograms normal mammary fibroblasts to promote inflammation and tumor growth in breast cancer. *Cancer Res* 2015, *75*, 963-973, doi:10.1158/0008-5472.Can-14-1990.

51. Sato, N.; Maehara, N.; Goggins, M. Gene expression profiling of tumor-stromal interactions between pancreatic cancer cells and stromal fibroblasts. *Cancer Res* 2004, *64*, 6950-6956, doi:10.1158/0008-5472.Can-04-0677.

52. Augsten, M. Cancer-associated fibroblasts as another polarized cell type of the tumor microenvironment. *Front Oncol* 2014, *4*, 62, doi:10.3389/fonc.2014.00062.

53. Alkasalias, T.; Moyano-Galceran, L.; Arsenian-Henriksson, M.; Lehti, K. Fibroblasts in the Tumor Microenvironment: Shield or Spear? *Int J Mol Sci* 2018, *19*, doi:10.3390/ijms19051532.

54. Kalluri, R. The biology and function of fibroblasts in cancer. *Nat Rev Cancer* **2016**, *16*, 582-598, doi:10.1038/nrc.2016.73.

55. Iacopino, F.; Angelucci, C.; Sica, G. Interactions between normal human fibroblasts and human prostate cancer cells in a co-culture system. *Anticancer Res* **2012**, *32*, 1579-1588.

56. De Wever, O.; Demetter, P.; Mareel, M.; Bracke, M. Stromal myofibroblasts are drivers of invasive cancer growth. *Int J Cancer* **2008**, *123*, 2229-2238, doi:10.1002/ijc.23925.

57. Strell, C.; Paulsson, J.; Jin, S.B.; Tobin, N.P.; Mezheyeuski, A.; Roswall, P.; Mutgan, C.; Mitsios, N.; Johansson, H.; Wickberg, S.M.; et al. Impact of Epithelial-Stromal Interactions on Peritumoral Fibroblasts in Ductal Carcinoma in Situ. *J Natl Cancer Inst* **2019**, *111*, 983-995, doi:10.1093/jnci/djy234.

58. Sahai, E.; Astsaturov, I.; Cukierman, E.; DeNardo, D.G.; Egeblad, M.; Evans, R.M.; Fearon, D.; Greten, F.R.; Hingorani, S.R.; Hunter, T.; et al. A framework for advancing our understanding of cancer-associated fibroblasts. *Nat Rev Cancer* **2020**, *20*, 174-186, doi:10.1038/s41568-019-0238-1.

59. Albrengues, J.; Bertero, T.; Grasset, E.; Bonan, S.; Maiel, M.; Bourget, I.; Philippe, C.; Herraiz Serrano, C.; Benamar, S.;

Croce, O.; et al. Epigenetic switch drives the conversion of fibroblasts into proinvasive cancer-associated fibroblasts. *Nat Commun* 2015, *6*, 10204, doi:10.1038/ncomms10204.

60. Kisseleva, T.; Brenner, D.A. Mechanisms of fibrogenesis. *Exp Biol Med (Maywood)* 2008, *233*, 109-122, doi:10.3181/0707-mr-190.

61. Neufert, C.; Becker, C.; Türeci, Ö.; Waldner, M.J.; Backert, I.; Floh, K.; Atreya, I.; Leppkes, M.; Jefremow, A.; Vieth, M.; et al. Tumor fibroblast-derived epiregulin promotes growth of colitis-associated neoplasms through ERK. *J Clin Invest* 2013, *123*, 1428-1443, doi:10.1172/jci63748.

62. Wang, L.; Cao, L.; Wang, H.; Liu, B.; Zhang, Q.; Meng, Z.; Wu, X.; Zhou, Q.; Xu, K. Cancer-associated fibroblasts enhance metastatic potential of lung cancer cells through IL-6/STAT3 signaling pathway. *Oncotarget* 2017, *8*, 76116-76128, doi:10.18632/oncotarget.18814.

63. Pape, J.; Magdeldin, T.; Stamati, K.; Nyga, A.; Loizidou, M.; Emberton, M.; Cheema, U. Cancer-associated fibroblasts mediate cancer progression and remodel the tumouroid stroma. *Br J Cancer* 2020, *123*, 1178-1190, doi:10.1038/s41416-020-0973-9.

64. Steer, A.; Cordes, N.; Jendrossek, V.; Klein, D. Impact of Cancer-Associated Fibroblast on the Radiation-Response of

Solid Xenograft Tumors. *Front Mol Biosci* 2019, *6*, 70, doi:10.3389/fmolb.2019.00070.

65. Bordignon, P.; Bottoni, G.; Xu, X.; Popescu, A.S.; Truan, Z.; Guenova, E.; Kofler, L.; Jafari, P.; Ostano, P.; Röcken, M.; et al. Dualism of FGF and TGF-β Signaling in Heterogeneous Cancer-Associated Fibroblast Activation with ETV1 as a Critical Determinant. *Cell Rep* 2019, *28*, 2358-2372.e2356, doi:10.1016/j.celrep.2019.07.092.

66. Giusti, I.; Di Francesco, M.; D'Ascenzo, S.; Palmerini, M.G.; Macchiarelli, G.; Carta, G.; Dolo, V. Ovarian cancer-derived extracellular vesicles affect normal human fibroblast behavior. *Cancer Biol Ther* 2018, *19*, 722-734, doi:10.1080/15384047.2018.1451286.

67. Noh, K.H.; Jeong, A.J.; Lee, H.L.; Lee, S.H.; Yi. E.; Chang, P.-S.; Kwak. C.; Ye, S.K. Crosstalk between prostate cancer cells and tumor-associated fibroblasts enhances the malignancy by inhibiting the tumor suppressor PLZF. *Cancers.* 2020, 12, 1083.

# 국문 초록

전립선암은 남성에게 가장 흔하게 발병되지만 증상이 거의 없기 때문에 조기 발견이 힘들어 주의가 필요한 종양이다. 전이가 일어나는 단계로 진행될 경우 통증이 수반되어 발견을 하더라도 생존율이 초기 단계에 비해 현저하게 낮다고 보고되었다. 그렇기 때문에 전립선암의 전이를 억제하는 전략의 중요성이 대두되고 있으며, 조기 발견에 사용될 획기적인 타겟을 찾는 것이 중요하다. 이에 본 연구자는 종양 미세 환경에 있는 다양한 기질 세포에 의한 전립선암의 전이를 억제하는 기전을 분석하고자 하였다.

이 연구에서 전골수구 백혈병 아연 집게(PLZF) 발현이 STAT3가 과발현하는 높은 단계의 전립선암 환자 조직과 음의 상관관계를 보이는 것뿐만 아니라 환자의 예후에도 기여하는 것을 확인하였다. 또한 PLZF 발현억제는 종양의 성장을 증가시켰고, 세포 사멸을 억제하였으며, 전립선 암세포의 이동과 전이를 촉진시키는 것을 확인하였다. 전립선암에서 야누스 인산화효소-신호 변환 및 전사활성인자 3 (JAKs-STAT3)는 종양의 악성도와 관련이 있으며, 종양 미세 환경에 의해 증가된 STAT3 활성화는 종양의 증식, 생존, 진행, 및 전이를 촉진시킨다는 연구결과가 보고되었다. 이러한 STAT3를 억제한다면 전립선 암뿐만 아니라 전반적인 종양 치료에 획기적인 전략이 될 것이다.

그런데 PLZF는 전사 인자임에도 불구하고 발암유전자인 STAT3의 전사를 조절하지 못하고 타이로신 인산화만을 감소시키는 것에 의문점이

생겼다. 따라서 전립선암 세포주에서 PLZF는 야누스 인산화효소(JAKs)-STAT3의 인산화를 감소시키는 타이로신 인산분해효소와 관련이 있을 것이라는 가설을 세웠다. 결과적으로 PLZF는 여러 가지 타이로신 인산분해효소 중 SHP-1의 전사인자로써 역할을 하여 JAKs-STAT3 기전을 억제하는 새로운 조절자 역할을 입증하였다. 이러한 결과는 PLZF와 마찬가지로 SHP-1 또한 전립선암 환자 조직에서 예후와 연관되어 있음을 보여줌으로써 확인하였다.

나아가, 종양 미세 환경의 기질 세포와 전립선 암세포의 상호작용을 통해 종양억제유전자인 PLZF가 전립선암에서 억제 되어있는 이유를 찾고자 하였다. 암세포와 섬유아세포 간에 신호전달물질의 교환을 통해 섬유아세포 유래 C-C 모티브 케모카인 리간드 3 (CCL3)에 의한 PLZF 발현 억제를 확인하였고, 이를 통해 전립선 암세포의 이동 및 전이 특성을 가속화함을 입증하였다.

결론적으로, 전립선 암세포는 종양미세환경의 섬유아세포와 상호작용을 통해 STAT3 활성화와 종양세포의 악성도가 증가하고, 이를 PLZF가 SHP-1을 통해 타이로신 인산화를 억제함으로써 암세포를 저해하는 새로운 치료 전략이 될 수 있음을 시사하였다. PLZF가 전립선암의 치료에 있어서 획기적인 표적이 될 수 있을 것을 기대한다.

---

**주요어 : 전골수구 백혈병 아연 집게, 타이로신 인산분해효소 1, 야누스 인산화효소-신호 변환 및 전사활성인자 3, 전립선암, 섬유아세포, 종양억제유전자**

**학 번 : 2014-21996**